Journal of Environmental Radioactivity 256 (2023) 107038

Contents lists available at ScienceDirect

Journal of Environmental Radioactivity

journal homepage: www.elsevier.com/locate/jenvrad

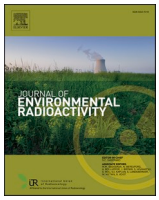

Vegetation induced distinctions between radionuclide distribution in soils (Austria)

Elisabeth Chr. B. Gottschling [a], Herbert Lettner [a,*], Alexander Karl Hubmer [a], Arnulf Schiller [b]

[a] Radiological Measurement Laboratory (RMLS), Biological Physics, Department of Chemistry and Physics of Materials, PLUS Salzburg University, Hellbrunnerstrasse 34, 5020, Salzburg, Austria
[b] Department of Geophysics, Geological Survey of Austria, eulinggasse 38, 1030, Wien, Austria

ARTICLE INFO

Keywords:
Depth distribution of radionuclides
Categorization in meadows and forests
Algorithm based on ternary diagrams

ABSTRACT

In 2019 and 2020, the layers - down to a maximum depth of 30 cm - of 43 soil samples from different regions in Austria were measured gamma-spectrometrically to determine their activity concentration (in Bq/kg and Bq/m^3) of ^{234}Th, ^{214}Pb, ^{214}Bi, ^{210}Pb, ^{228}Ac and ^{40}K. ^{137}Cs activity concentration (in Bq/m^3) will be found in the supplementary data file only. A basic statistical analysis was carried out and explained variances for distinctions primarily between meadows and forests. Ternary diagrams were applied to represent equilibrium status of inventories and layer activities between ^{238}U-equivalent, ^{226}Ra-equivalent and ^{210}Pb. A method using ternary diagrams for identifying of element-specific dampening effects in remote sensing is presented in the report (ternary "adjustment" diagrams).

The tendencies between forest and meadows sites are heterogeneous, but distinctions between coniferous and deciduous forest are extremely likely. Geological settings dominate the distributions, slightly altered by anthropogenic influence, which includes the kind of vegetation. Focusing on top soil layers (first and/or second layer) facilitates discrimination according to vegetation. At some sites changes of activities in the grass root layer (at 15 cm) were observed.

1. Introduction

This study on radionuclide distribution in soils was carried out at the Geological Survey of Austria (MRI-VEGAM, Multidisciplinary study for determination of accurate vegetational and topographic correction of airborne gamma-ray spectrometry data by means of an UAV measurement system). Airborne gamma-ray spectrometry is one of the most elegant and effective options for prospecting mineral resources (Minty, 1997). However, it requires unadulterated data with maximum information content as possible to obtain quality indirect information on geochemistry and lithology in the study area. This requires careful post-processing and correction of the data.

The gamma field, the photon flux that penetrate the detector in the plane, helicopter or drone, is primarily produced by the gamma-emitters of the ^{238}U, ^{235}U and ^{232}Th decay chain and ^{40}K in the soil (the inventory, ground truth or source term) in the soil or rock underneath the flying object. To a minor extent radon decay products in the atmosphere and cosmic radiation contribute to the gamma field and in fallout contaminated regions, artificial radionuclides such as ^{137}Cs may as well contribute depending on the level of contamination. Due to attenuation and absorption of the emitted gamma-photons the maximum thickness even for high energy photons of the natural radionuclides that are prospected, is limited to 20 –30 cm soil depth. Any radionuclides below this depth cannot be detected by airborne gamma-ray spectrometry (IAEA TECDOC 1363, 2003; Minty, 1997).

The photon flux above ground penetration the detector is at first order a function of the inventory of the radionuclides in the soil, its spatial and vertical (depth) distribution, the soil density and the water content in the soil. In case of vegetation cover, damping by vegetation may have a great influence and has to be considered for data processing. Soil density and soil water content are closely linked to climatic conditions and both variables show a strong depth profile. Physical chemical processes including sorption and desorption may result in shifting of the vertical concentration of certain elements, which can also affect natural radionuclides and may finally lead to inhomogeneous vertical depth distribution. The shape of the depth profile is particularly

* Corresponding author.
E-mail addresses: gottschling@aon.at (E.Chr.B. Gottschling), herbert.lettner@plus.ac.at (H. Lettner), Alexander.hubmer@plus.ac.at (A.K. Hubmer), arnulf.schiller@geologie.ac.at (A. Schiller).

https://doi.org/10.1016/j.jenvrad.2022.107038
Received 10 December 2021; Received in revised form 13 September 2022; Accepted 29 September 2022
Available online 4 November 2022

important for radionuclides such as ^{137}Cs deposited by fallout at the soil surface and which reshapes by migration into deeper soil layers resulting in reduction of the photon flux. In airborne gamma-ray spectrometry, natural radionuclides are assumed to be uniformly distributed along depth in the soil (Minty, 1997), however this might be far from reality. Detailed knowledge of the depth distribution on the gamma-emitters analyzed, the soil density profile and the soil water content are thus crucial for the quantitative analysis of the gamma spectrum obtained by airborne gamma-ray spectrometry and the calculation of the inventory of uranium (U) and other radionuclides.

The objective of this study was to collect data on the depth and spatial distribution of the gamma-emitters in the ^{238}U and ^{232}Th decay chains and of ^{40}K on selected test sites. Three sites were selected, each site roughly of 200 m × 300 m in size, situated in a different geological unit and approximately half of the area used as meadow or pasture and the rest of the area forested.

These three sites are part of a larger set of eight study sets selected in course of the host-project MRI-VEGAM in order to generate a dataset as a base for systematic analyses of vegetational and topographic effects on airborne gamma-ray spectrometry. In context of the host study, the radionuclide inventories of these three sites provide crucial ground truth data, whereas all sites were selected following the goal to cover a representative spectrum of characteristics, i.e. type of vegetation and seasonal variation, geological units with different levels and spectra of radio-activity, different types of topography (simple to distinct), existing information on geology and geophysics (i.e. existing mapping, airborne and ground geophysics data), and accessibility for drone surveying.

The selection criteria were applied in order to test the hypothesis of uniform distribution of natural radionuclides in the soil profile in general and to determine systematic differences between the inventory of grass covered and forest covered soil, which could cause a potential bias in the interpretation of airborne gamma-ray spectrometry. Parallel to vegetational criteria, lithology has been considered spanning from granitic units of higher activity (Pengers) with thin soil cover over mica schist and phyllitic units (Heuberg) to mainly glacial/alluvial sedimentation with lower activity (Sötz).

At three locations, in Pengers, Heuberg and Sötz (all within a radius of 150 km from Vienna/Austria), 12, 16 and 15 soil cores were extracted a. Data evaluation focused on a comparison between soil samples taken from meadows and those taken in forests. Statistical values of the mass- and volume-specific inventories were calculated and the explained variance for these categories computed (by a specially designed VBA (Visual Basic for Application) code for Excel). The explained variance was used instead of F-value or level of significance because the variances of the activities in the categories are not equal (within acceptable ranges) in most cases. The explained variance is the fraction of the sum of sums of squared deviations within in the categories with regard to the sum of squared deviations for the total sample (a formula is found in Appendix A). The higher the explained variance the more favorable the categories. In addition, the explained variance for other arrangements in groups tested the best categorization.

The depth distributions of the measured radionuclides and their dependency on soil density are discussed.

Ternary diagrams are used to represent the secular equilibrium status of the samples. Most likely geological specialties and the human use are found to be the major causes for disequilibria.

The use of another type of ternary diagram for ^{214}Bi - ^{228}Ac - ^{40}K is presented to compare soil samples with surface data derived by aero-gamma-spectrometric measurements by drone (or scanner) and to calculate correction factors for each radionuclide in the proper environment.

2. Data acquisition

2.1. Material and methods

2.1.1. Soil sampling and preparation

Soil samples were taken with a soil corer of 8.1 cm diameter and 15 cm core length. On meadows the grass was cut 1–2 cm close to the soil prior to sampling and in forests the litter was removed. The corer was driven into soil with a dead blow hammer, then the soil core was removed and another core sampled from the same hole to obtain a total core length of roughly 30 cm. In the field, the soil cores were pushed out of the corer with a piston directly into a Plexiglas tube of slightly greater diameter than the corer, to make sure the soil core was inserted in such a way as to keep its structure intact for storage and transport.

In the laboratory the soil cores were sliced into 3 cm layers at Pengers, and into 5 cm layers at the other. In a drying chamber the samples were dried at 105 °C for at least 24 h until constant weight to determine the soil density. To prepare for gamma spectrometry the dried soil was crushed and ground in a mortar with a pestle to homogenize the material. From the homogenized sample a quantity of between 60 and 600 mL was placed into a polyethylene container, weight and volume determined and the lid of the container welded with the housing to make it gas tight and prevent ^{222}Rn from escaping.

2.1.2. Gamma spectrometry

In this closed system, after 3 weeks ^{226}Ra comes into equilibrium with ^{222}Rn and its short-lived decay products, ^{218}Po, ^{214}Bi and ^{214}Pb. The latter two are readily measurable with gamma spectrometry and allow for the indirect determination of ^{226}Ra, whose direct measurement is rather uncertain due to low emission probability and interference with gamma energies of ^{235}U. The other gamma-emitting radionuclides of interest in the ^{238}U decay chain, ^{234}Th und ^{210}Pb, were measured directly by low-energy gamma lines. Among the other natural radionuclides, ^{228}Ac was measured at 911 keV, assuming equilibrium with its parent ^{232}Th, and the single radionuclide ^{40}K was determined directly by its 1460 keV high energy gamma line.

Due to low self-absorption in the sample, the high energy gamma range is not problematic and the data are rather accurate; however, in the low energy range of ^{210}Pb and ^{234}Th (for ^{238}U) the results are less accurate. The total uncertainty for the mid and high gamma energy measurements (^{214}Bi and ^{214}Pb for ^{226}Ra, ^{4} K, ^{232}Th, ^{137}Cs) is estimated in the range between 5% and 15% and the uncertainty for the low energy data of ^{210}Pb and ^{234}Th (for ^{238}U) is between 10% and 20%. Low total uncertainties of 5% can only be reached for ^{137}Cs – a single peak radionuclide. Detector equipment used were HpGe detectors with efficiencies between 30% and 40%. Detector calibration was done with radionuclide standards in the geometries used for measurement, and good laboratory practice and quality assurance of the results is certified by the regular participation on national and international intercomparison exercises.

2.2. Site information

All three sites were subdivided into meadows and forest both more or less equal in size. The meadows are used for grass and hay production and cut twice a season. Fertilization is only occasionally done at Pengers, and restricted to applying manure. Seasonal grazing of sheep may occasionally occur at Sötz/Weyer (all information retrieved from land users).

Site 1, *Pengers*: Pengers is in Lower Austria on the granite and gneiss plateau locally consisting of Eisgarner Granite (Berka et al., 2014, p.74). The sample location covers a rectangular area of 200 m by 300 m. The distances between sample sites are 100 m. 12 samples were taken from Pengers in winter of 2019, 6 were in meadows and 6 in coniferous forest (spruce). Pengers meadow is a hanggley soil type on a slight slope to a pond and a G_r-horizon beginning at about 15–20 cm of depth (eBOD2,

2020). The meadow is composed of two types of fields with different soil densities in the topsoil, the upper field near the forest, the other near a pond. Maximal average slope between two sites is 6° to the west. Site 2, *Heuberg*: In summer of 2020 16 samples were taken in Heuberg (near the castle Forchtenstein). The "Rosalien" mountains are the easternmost part of the central eastern Alps south the Vienna basin. Of the samples, 6 were located on the meadow, 6 in the forest and 4 in an area which suits both and is called "border area". One site of the border area in Heuberg was a deforested area with young conifers and wild undergrowth, another a narrow glade, the third and the fourth were near young conifers and one of these sites was near an anthill (within 5 m). All sites of the border area were downhill, while most of the meadow sites were uphill, with the forest sites in between. Slopes ranged between 1° and 17° in reference to the highest sample site. Only one sample was located on a plateau (H5). The sample locations were more irregularly distributed on an area of 5 ha due to topographical restrictions. Soil type information is available on the website "Standortskarte" cited in the bibliography. Site 3, *Sötz/Weyer*: In fall of 2020 15 samples were extracted in Sötz near Weyer in the northern limestone Alps after a rainy weather period. 6 samples were situated in meadows, 7 in forests and 2 in or near a gravel pit. Holocene valley filling and the Opponitz formation on higher grounds (Pleiderer et al., 2002; page 48) were detected. Slopes varied between 5° and 15°. Site locations varied slightly from regular grid covering 4 ha due to topography.

The sample sites were located between 500 and 700 m (above sea level).

3. Results and discussion

3.1. Statistics for soil (bulk) densities

Soil bulk density (in Fig. 1) in general depends on vegetation type and topography. In Pengers a coniferous forest with a low slope leads to low densities in the topsoil layers. As erosion is low, the litter stays local and takes a long time to rot. The appearance of meadow densities in Pengers is twofold. Dense top soil near the forest, which is supposed to be a regular field, and lighter top soil densities from the samples nearer to the pond. An anthropogenic influence on soil compression by tractors can be assumed. After an increase to a depth of 15 cm in Heuberg and 10 cm in Sötz the soil density remains constant with small deviations. The increase is stronger in sites populated by coniferous trees.

In Heuberg and Sötz the total layers of the samples had not been measured gamma-spectrometrically only a part of each layer. This causes two different measures of soil densities, a soil density of the total sample layer (called "total density") and a soil density of the gamma-spectrometrically measured part of the sample layer (called "measure density") (see inventory formulas in appendix C). Deviations are caused by the double extraction (separated at 15 cm), missing parts of the end sector, stone and roots.

3.2. Radionuclide ^{234}Th ($^{238}U^{e1}$)

The deviations of mass-specific and volume-specific inventories of ^{238}U daughter radionuclide ^{234}Th (mass-specific inventories in Fig. 2) between meadow and forest were small in Heuberg and Sötz. Samples located in a border area between meadow and forest in Heuberg showed lower ^{234}Th inventories of both types than the average in Heuberg. These sites will be addressed together with ^{226}Ra in the next section.

In Pengers meadow an extreme spike near the pond (in P8) was measured, coinciding with much lower soil density in this sample. The mass-specific inventory of ^{238}U-equivalent in Pengers P8 is nearly ten times higher than in most other samples. Without this sample the mass-specific inventory will decline from 0.176 to 0.110 Bq/g. Taking possible measurement uncertainties into account, a clear minimal difference of 0.0376 Bq/g between forest and selected meadow for averaged mass-specific inventories remained. Either the activity of ^{234}Th in Pengers forest was systematically lower or the activity in the meadow of Pengers was systematically higher depending on the reference point to be determined.

In Pengers ^{234}Th was nearly in equilibrium with ^{226}Ra in the meadow samples but not in the forest samples (ternary equilibrium diagram in Figs. 3 and 4). Choosing equilibria as reference point, which are rare in

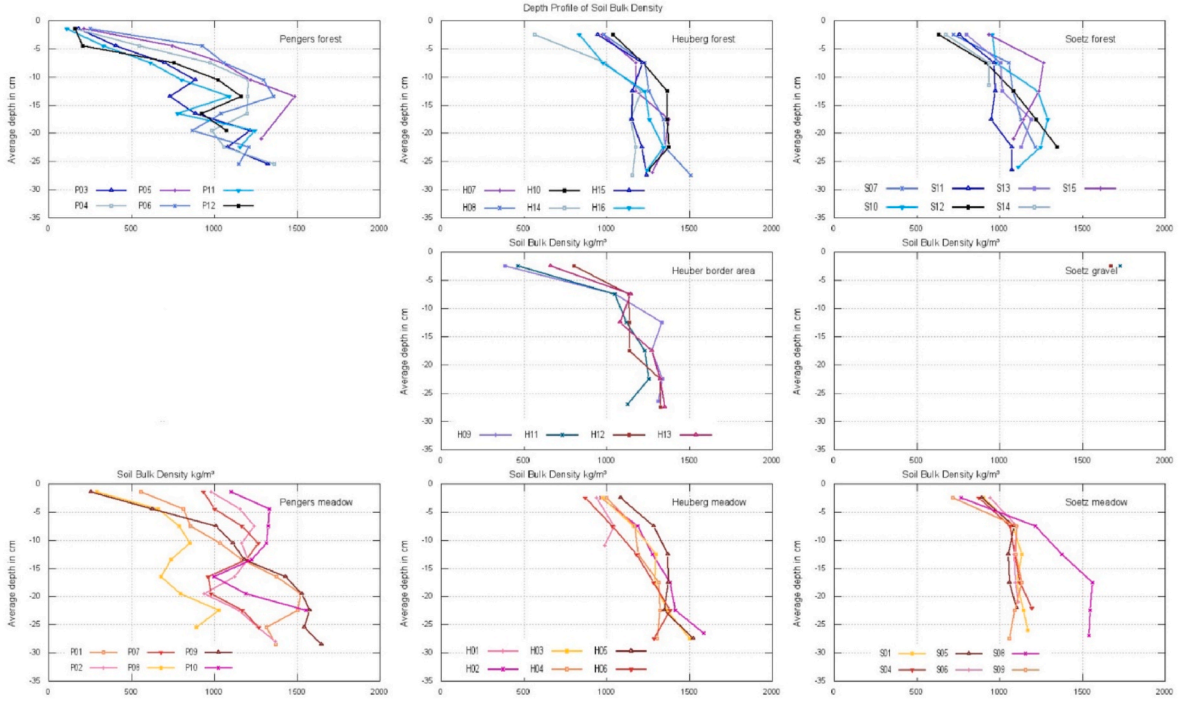

Fig. 1. Depth profile of the soil bulk density of the radiologically measured part of the sample separated according to the site location – Pengers – Heuberg – Sötz and the quality meadow, forest, border aera/gravel.

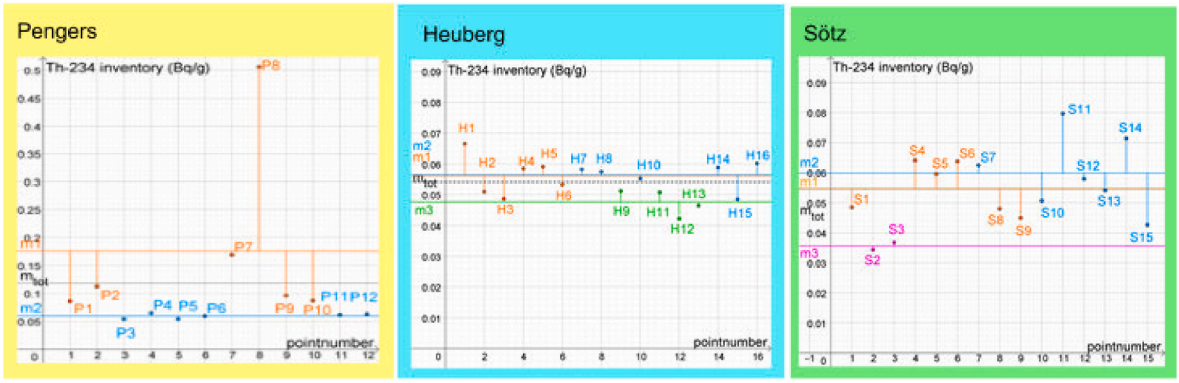

Fig. 2. Mass specific inventory of ^{234}Th for Pengers, Heuberg and Sötz. Orange points represent meadow values, forest in blue, borderarea in green and gravel in pink. Horizontal line are associated mean values. Note: the scaling differs from figure to figure. (For interpretation of the references to colour in this figure legend, the reader is referred to the Web version of this article.)

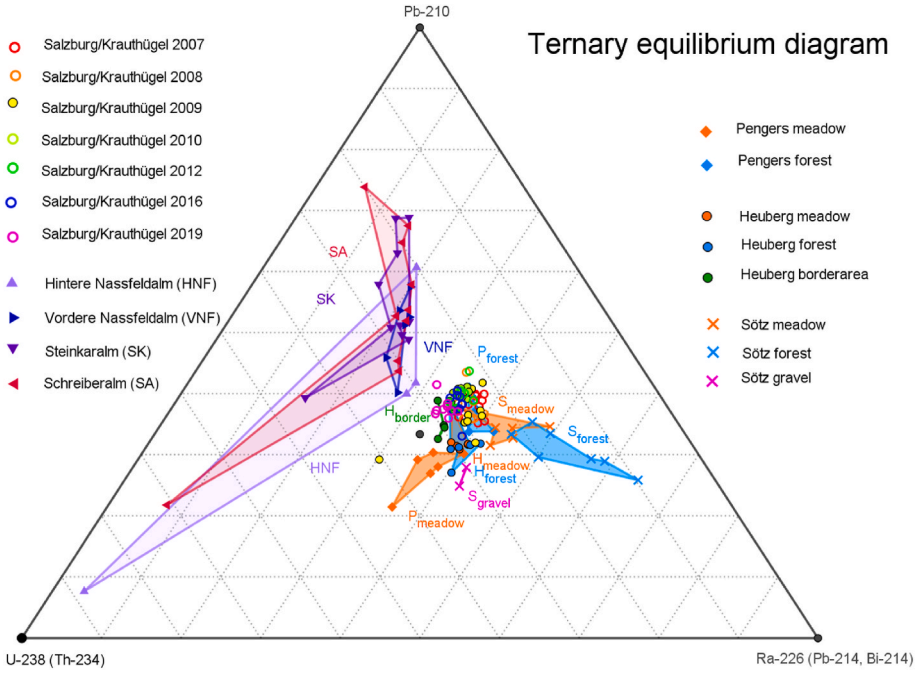

Fig. 3. Ternary equilibrium diagram for mass-specific inventory – overview.

open systems in nature, a depletion of ^{234}Th in the forest can be considered. The depletion imbalance in Pengers was not exclusively caused by a first layer sink in the forest, but was present throughout the profile. According to literature the content of soil organic matter (SOM) is relevant for plant uptake (Morton, 2002), and forest soil, at least in the top 15 cm, usually contains more SOM (different in Navas et al., 2011). Thørring et al. (2020) measured in a small number of sites that the activity concentration (in Bq/kg) of ^{238}U in soil from grass-dominated sites is higher than those from birch forests (in Norway). Similarly Ahmed et al. (2014) observed higher values of U in arable surface soil layers than in underlying soil layers or woodland soil.

For higher ^{234}Th concentrations on cultivated meadows, phosphate fertilization may be assumed. Takeda (2006) (in Ahmed et al., 2014; in Vukašinović et al., 2010; Harmsen and de Haan, 1980) reported a strong influence of SOM and non-crystalline clay minerals on accumulation and enrichment of U derived from phosphate fertilizers (in humus rich andisols).

The grass of Pengers meadow was harvested implying continuous removal of potassium. But the ^{40}K activity is only slightly under the level of the forest (for relation of ^{40}K and K see Fujiyoshi et al., 2014). A fertilization with potassium most likely implied a fertilization with phosphate as well. A long-term application of phosphate fertilizers could elevate primordial radionuclide concentrations (^{40}K, ^{238}U, ^{232}Th) in the surface soil layers (MortVedt, 1994; Takeda, 2006; Falck, 2006; as all cited in Vukašinović et al., 2010). Less mobile ^{228}Ac was indeed elevated in the topsoil layer in Pengers meadow near the forest. Plowing as indicated by the constant distribution of the activity concentration (in Bq/m^3) of ^{137}Cs and ^{210}Pb in the soil under Pengers meadow near the forest could have spread the radionuclides especially ^{234}Th evenly down to 15 cm depth. Harmsen and de Haan (1980) calculated it would take 30 years of phosphate fertilization to increase the U content of the soil by 1 mg/kg (1 ppm ^{238}U~12.4 Bq/kg ^{238}U). This magnitude would hold for the difference found between neighboring meadow and forest sites in the Sötz inventories but not for Pengers inventories of forest and meadow differing by 117 Bq/kg on average. In Pengers meadow a hydromorphic soil is assumed based on topography, soil type, density and distribution of activity concentration (in Bq/m^3). Gueniot et al. (1988) describes the depth distribution of U in hydromorphic soils, where topography and water table as local factors for migration are essential. This implies enrichment of U down the slope in hydromorphic soils in

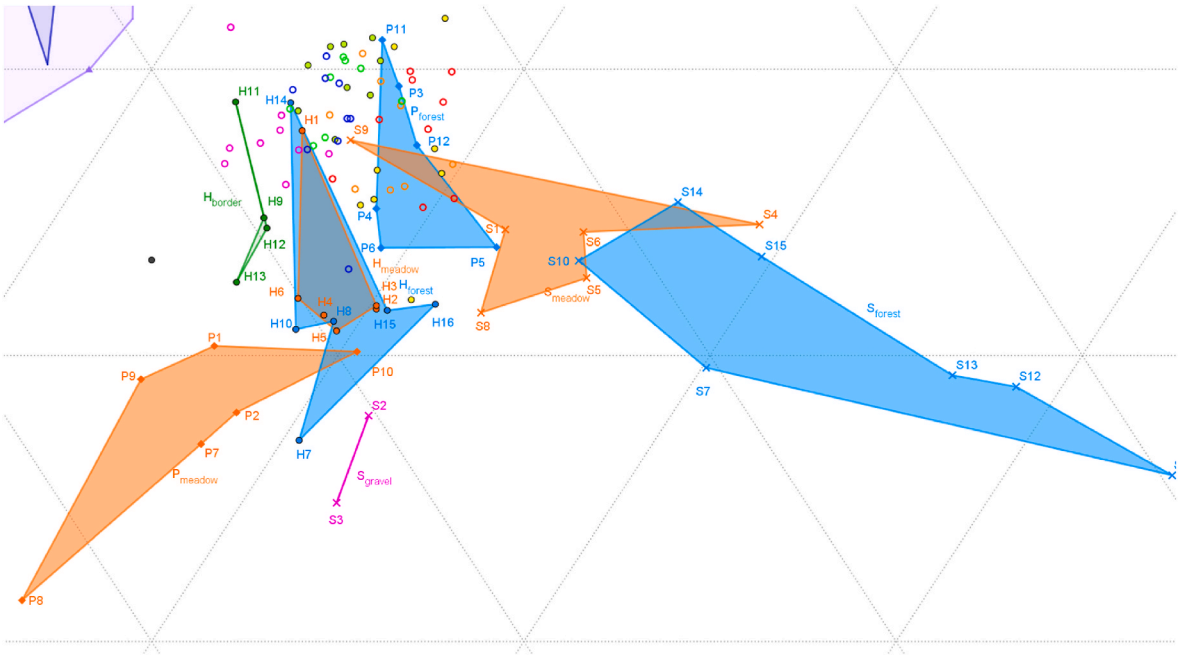

Fig. 4. Ternary equilibrium diagram for mass-specific inventory - detail with polygon areas and single denotation (legend in Fig. 3).

comparison to those in a plain (Gueniot et al., 1988). He assumed U accumulation in organic-rich and reduced horizons, especially the U migration from a G_o to a G_r-horizon promoted by water table fluctuations were discussed in Gueniot's article. Most likely phosphate fertilizer and mechanical mixing in combination with a hydromorphic soil establish an equilibrium situation in the soil under Pengers meadows, where the disequilibria in forests appeared to be an undisturbed situation for a relatively closed system.

Explained variances for ^{234}Th were calculated. For volume-specific inventories 41% in Pengers, 59% in Heuberg and 0.02% in Sötz of the deviation could be explained with a categorization by vegetation, although the high explained variance in Heuberg is caused by lower activity in the border area. Mass-specific inventories show 23% in Pengers, 38% in Heuberg and 41% (caused by a third category "gravel") in Sötz explained variance.

The explained variances of layers in Pengers and Heuberg show better (higher) values in layers above 15 cm (root zone).

Higher values for explained variances were achieved by other categorizations, for example in Pengers, when the meadows are separated in near forest and near pond. In Heuberg vegetation type categories seem the best (tested against a "location" and "soil" categorization). The samples in Sötz are heterogeneous. By categorizing according to an "assumed soil" type based on neighboring locations and/or hill slope higher explained variances were achieved for volume-specific inventory and most layer activity concentration (in Bq/m^3) in Sötz. Mass-specific inventories provide better explained variances for categorization by vegetation type. Explained variances of activity concentrations (in Bq/kg) of categorization "soil" in layers are higher with the exception that of the top layer.

The relation of ^{234}Th activity concentration (in Bq/kg) (or activity concentration (in Bq/m^3)) and (measure) density is different based on the site. In some sites a convergence to the same limit from higher (Pengers meadow) and from lower (Pengers forest) values were observed for both kind of activities.

3.3. Average of ^{214}Pb and ^{214}Bi as ^{226}Ra^e

Some remote sensors use ^{214}Bi or ^{214}Pb for approximation of the activity concentrations (in Bq/kg) of ^{238}U. Therefore ^{226}Ra^e as the average of ^{214}Pb and ^{214}Bi will suit for comparison with the remote data for ^{238}U^{e2}.

Most sample values ranged between 60 and 120 Bq/kg of mass-specific inventory for ^{226}Ra^e (see Fig. 5).

The depth distribution of radium was definitely parallel to the ^{234}Th depth distribution in all sites in Pengers; for most sites in Heuberg and only a few sites in Sötz. Sötz forests showed an abundance of radium in comparison with managed meadows in Sötz and especially with the other sites.

The given data showed an unresolved effect on the dependency between altitude and the mass-specific inventory of ^{226}Ra^e. In Heuberg and Sötz the slope of the regression line of mass-specific inventory of ^{226}Ra^e versus altitude was positive. In Pengers a hydromorphic soil in connection with a field fertilization is supposed to cause the negative correlation for meadows only. The highest ^{226}Ra^e mass-specific inventory was measured at the lowest location (P8). Without it the correlation coefficient would be +0.56. In Sötz the forest samples are supposed to be part of the Opponitz formation, which could be an additional cause of the high values in the forest. The samples from the border area in Heuberg showed the lowest ^{226}Ra^e mass-specific inventories. Their location in the ternary equilibrium diagram (Figs. 3 and 4) was the nearest to equilibrium in reference to radium and U for all samples from Heuberg. Heuberg border area site H11 was settled near an anthill. Anthills often indicate ascending carbon dioxide. The CO_2-content of soils may depend on the biological activity and influences the formation of uranyl-carbonate complexes and therefore increases the solubility of U in natural waters (Harmsen and de Haan, 1980; Sharma et al., 2018). Harmsen and de Haan (1980) explain, if "*the CO_2 pressure in the top soil is higher than at depth, U could dissolve in the top soil, leach downwards and precipitate again at depth, because of the lower CO_2 pressure*". He concluded, for "*the solubility and mobility of U in soil local conditions of* pH *and CO_2 content have to be taken into account*". Leaching of U because of CO_2-content could leave (relatively) excessive concentration of radium behind or reduce the activity of all radionuclides of this series.

In sites at lower altitude the biological activity was most likely higher than in sites at higher altitude. As a consequence lower activities of ^{234}Th and ^{226}Ra at lower sites are more likely.

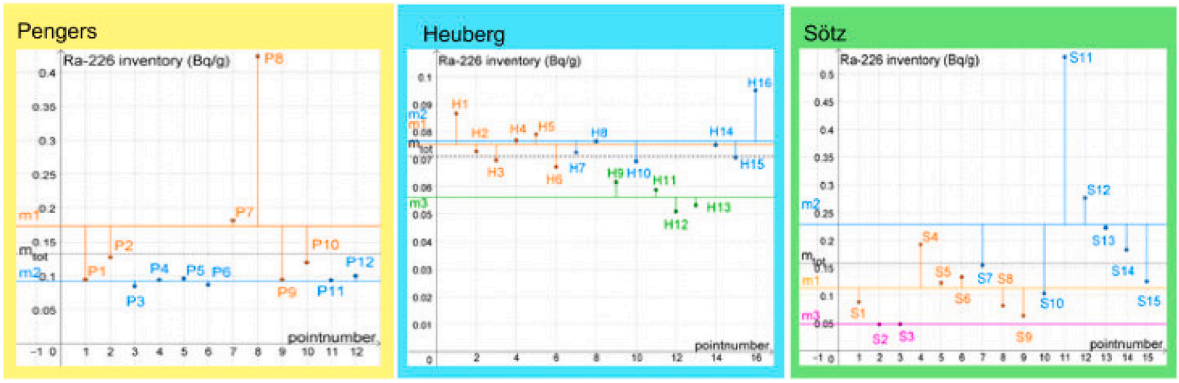

Fig. 5. Mass specific inventory of ^{226}Ra for Pengers, Heuberg and Sötz. Orange points represent meadow values, forest in blue, border area in green and gravel in pink. Horizontal line are associated mean values. Note: the scaling differs from figure to figure. (For interpretation of the references to colour in this figure legend, the reader is referred to the Web version of this article.)

3.4. Radionuclide ^{210}Pb

The observed ^{210}Pb activity reflected the endogenous and the atmospheric contribution in the top layers. Excess lead (^{210}Pb$_{exc}$) reduces with depth which is shown visually in the ternary equilibrium diagrams of the soil layers (Figs. 6–9). There is an obvious distinction between volume-specific inventories of ^{210}Pb of meadow and forest in Pengers and Sötz (explained variance 44% and 41%) but not in Heuberg (explained variance 14%) (Mass specific inventories are found in Fig. 10). The amount of the explained variance in each soil layer varied across the profile due to two causes. In top soil the density of the vegetation and the vegetation period effects enrichment. Coniferous forest could intercept aerosols in the winter season, too. All but two meadows in Heuberg were uncut (H1 and H5) and the understory in the beech forest was rare (H8, H10). He and Walling (1997) derived an exponential decrease of ^{210}Pb activity concentration (in Bq/kg) with depth in uncultivated soils and a constant distribution in plowed soils due to mechanical mixing. Therefore, plowing could be assumed at least partly for Pengers meadow via ^{210}Pb (and ^{137}Cs) depth distribution, although the depth distributions show different slopes for the three sites. A more coherent view is provided by the dependency on soil density. For all layers the activity concentration (in Bq/kg) is observed to decrease exponentially with (total and measure) density (Figs. 11 and 12). Three auxiliary exponential decrease functions with an offset and half-densities of 200, 250 and 350 kg/m^3 gives a lower bound, an upper bound and an untechnical approximate: f1(x) = 25 + 800 × 0.5^(x/200); f2(x) = 25 + 1000 × 0.5^(x/350); f3(x) = 25 + 900 × 0.5^(x/250).

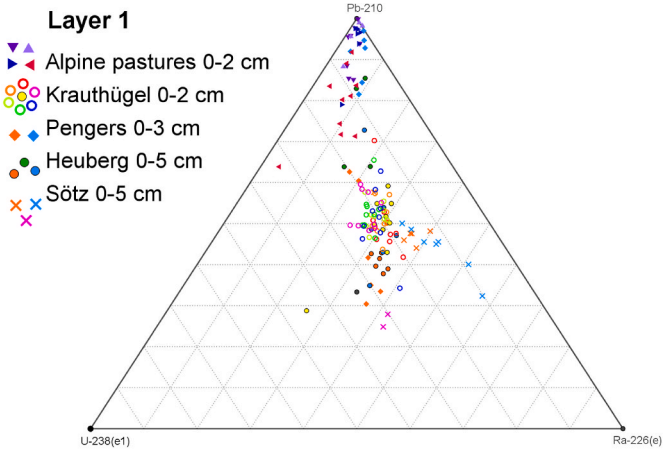

Fig. 6. Ternary equilibrium diagram for layer 1 (see also legend in Fig. 3).

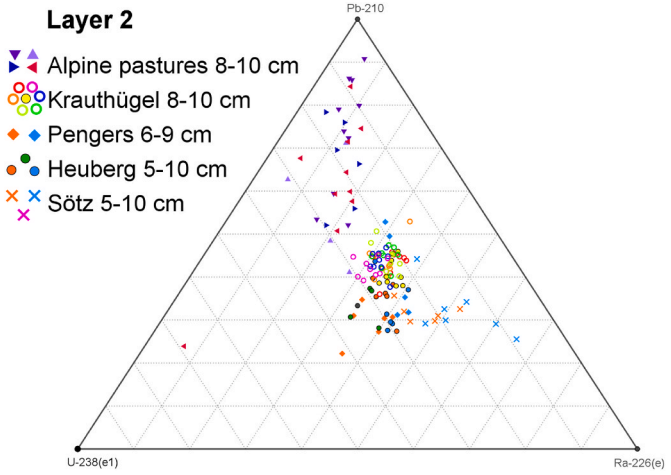

Fig. 7. Ternary equilibrium diagram for layer 2 (see also legend in Fig. 3).

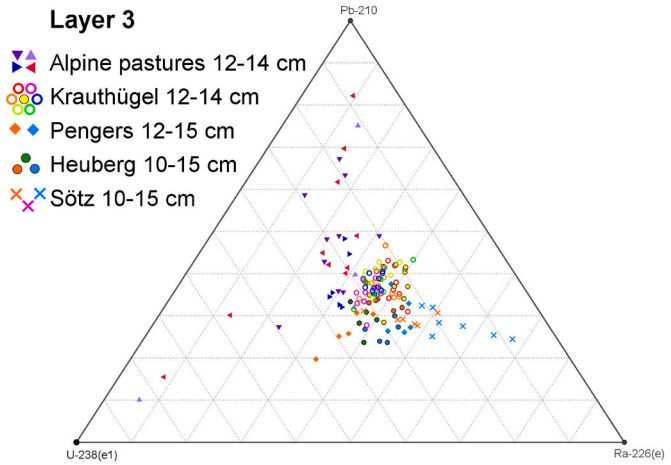

Fig. 8. Ternary equilibrium diagram for layer 3 (see also legend in Fig. 3).

3.5. Radionuclide ^{40}K

Anthropogenic causes of increased ^{40}K concentration near human villages or economic regions (Charlesworth, 2011 as cited in Vukašinović et al., 2018) compete with the mineralogical setting, "*where K-bearing primary minerals (Feldspar and mica) might show a downwards increase (in a forest soil), because ^{40}K accommodation in crystal structure is*

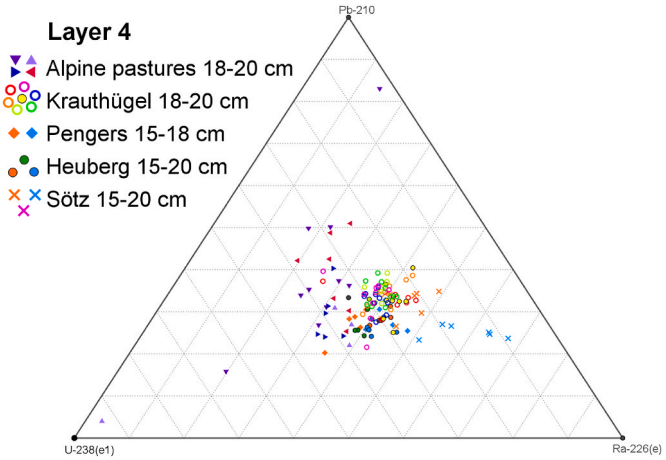

Fig. 9. Ternary equilibrium diagram for layer 4 (see also legend in Fig. 3).

better than that of U or thorium (ionic radius)" (Baeza, 1995 as cited in Scarciglia et al., 2020).

In Pengers ^{40}K activity concentrations (in Bq/kg) stagnated after a sharp increase in forest samples with depth, in meadows sampled a twofold behavior with depth (rising and constant) coinciding with soil density were observed. Heuberg border area resembled Pengers forest while meadow and forest in Heuberg did not differ significantly. Sötz samples showed great local diversity in their depth distribution of activity concentrations (in Bq/kg). Please see the figures in the supplementary data file.

A similarity of depth distribution patterns between ^{40}K and ^{226}Ra was not observed in the present data as mentioned in Fujiyoshi and Sawamura (2004) for forest soils. In Sötz a similarity between ^{228}Ac (^{232}Th^{e}) and ^{40}K was recognized. The spike in Pengers P8 is ambivalent, low ^{40}K and high ^{228}Ac activity are combined with low soil density.

In Pengers the trend between meadow and forest regarding dependence between activity concentration (in Bq/kg) and soil density is different. Forest samples in particular showed low activity concentrations (in Bq/m^3) in topsoil layers. After a steep increase they stagnated at 1000–1300 Bq/kg. Meadows started with higher values but reached only between 800 and 1100 Bq/kg in lower layers except for the spike in P8.

In Heuberg only regression lines give an impression of differences between meadows, forest and border areas concerning activity dependency on soil density. The average slope for meadow samples was 0.08 and 0.29 (in Bq m^3/kg^2) in forest ones for activity concentration (in Bq/kg). Border area values resembled Pengers forest ones, indicating conifer population. H15 and H16 settled in an alluvial channel have the lowest activities in comparison to the other forest samples on a nearly constant level.

Activity concentrations (in Bq/kg) in Sötz are generally lower than activity concentrations (in Bq/kg) in Pengers or Heuberg. All regression lines had a negative slope here. It seems there is no K bearing rock in the underground. Highest values in Sötz were measured in samples from a cow pasture (S5 and S6), the proximity (of values and location) to one forest sample (S7) indicates a local condition.

In literature data of soil samples, the activity concentration of ^{40}K is positively correlated with an increasing soil density (Fujiyoshi and Sawamura, 2004; Nenadović et al., 2012). In the samples from Heuberg ^{40}K activity concentration (in Bq/kg) correlated with measure density with a correlation coefficient $r_{total} = 0.37$ ($r_{forest} = 0.44$, $r_{meadow} = 0.14$, $r_{border\ area} = 0.79$), in Pengers: $r_{total} = 0.69$ ($r_{forest} = 0.87$, $r_{meadow} = 0.77$) and in Sötz: $r_{total} = -0.41$, ($r_{forest} = -0.45$, $r_{meadow} = -0.42$), the correlation with total density was less pronounced.

^{40}K activity concentration (in Bq/m^3) in Pengers, Heuberg and most Sötz forest sites show an increase with depth, while activity concentration (in Bq/m^3) in many Sötz meadow sites stays nearly constant with depth.

Potassium shows different explained variances regarding volume (0.03% caused by P8 spike, without P8: 13%) or mass-specific (50%) inventories in Pengers, respectively in Heuberg 7% (vol.) and 41%

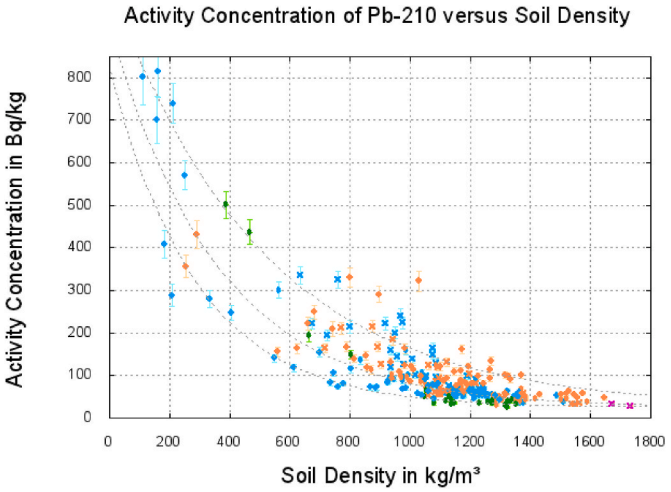

Fig. 11. Activity concentration (in Bq/kg) of ^{210}Pb vs. measure density and auxiliary exponential decrease curves (see legend in Fig. 3 or Fig. 12) Deviations of measure density are not presented in the figure. Average deviation of measure density is approximately 33 kg/m^3.

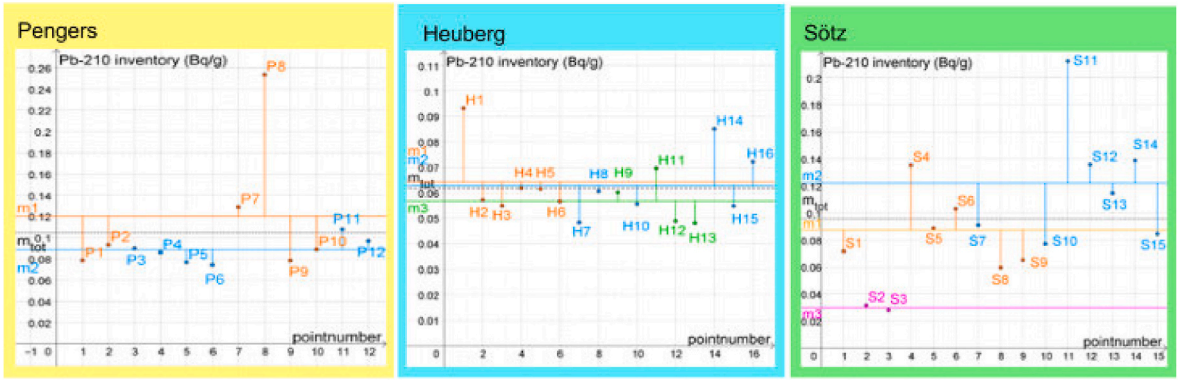

Fig. 10. Mass specific inventory of ^{210}Pb for Pengers, Heuberg and Sötz. Orange points represent meadow values, forest in blue, border area in green and gravel in pink. Horizontal line are associated mean values. Note: the scaling differs from figure to figure. (For interpretation of the references to colour in this figure legend, the reader is referred to the Web version of this article.)

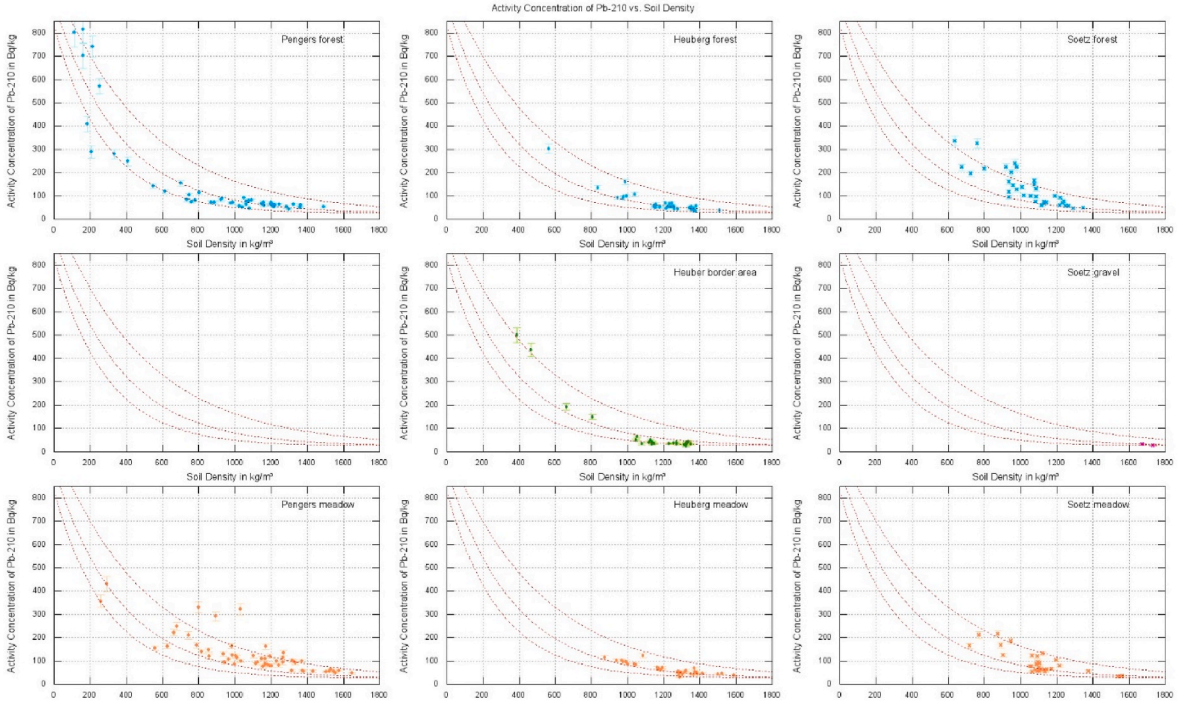

Fig. 12. Here the data points of Fig. 11 are separated according to site location and vegetation category. Note: The central figure in the column for Pengers contains no data points. There are only two categories in Pengers.

(mass) and in Sötz 32% (vol.) and 34% (mass). The first or second layer showed higher explained variances, which could have greater influence on remote sensing results.

The explained variance for activity differences between layers "A (i+1) – A(i)" gave higher values in the grass root zone in Pengers and in the first layer in Heuberg. Sötz data showed only relatively higher explained variance for activity concentration (in Bq/m^3) (11%) in the grass root zone, while value are maximal 5% outside root zone.

Mass specific inventory of ^{40}K is represented in Fig. 13, all depth profiles – data and figures - may be found in an supplementary data file.

3.6. Radionuclide ^{228}Ac (^{232}Th^e)

In Pengers the depth profile of ^{228}Ac activities was similar to that of ^{234}Th, a bit lesser in Heuberg. In Sötz the activities' depth profiles for activities of ^{228}Ac were nearly parallel to the depth profiles of ^{40}K, but the deviation was smaller in the forest sites. The same holds for depth profiles of activity concentration in Bq/kg and Bq/m^3. Manigandan and Chandar Shekar (2017) reported a positive correlation between ^{232}Th and ^{238}U in their samples. This does not hold for the samples from Sötz which remain constant on different levels, perhaps due the genesis of the site. The folding of the Alps and weathering has brought different rock formation in a close proximity to surface.

As for ^{234}Th and ^{40}K the dependency of the ^{228}Ac activity on measure density was observed. Besides the P8 spike, a threshold of activity concentration (in Bq/kg) of 70–90 Bq/kg in the depth independent on soil density in the samples can be assumed. For activity concentration (in Bq/m^3) no threshold down to a depth of 30 cm was indicated.

In Heuberg a threshold near 60 Bq/kg (approached from above and below) held for activity concentration (in Bq/kg). Samples from border area and that in the alluvial channel (forest) approached from lower value, the other from higher values. This could be a local effect because

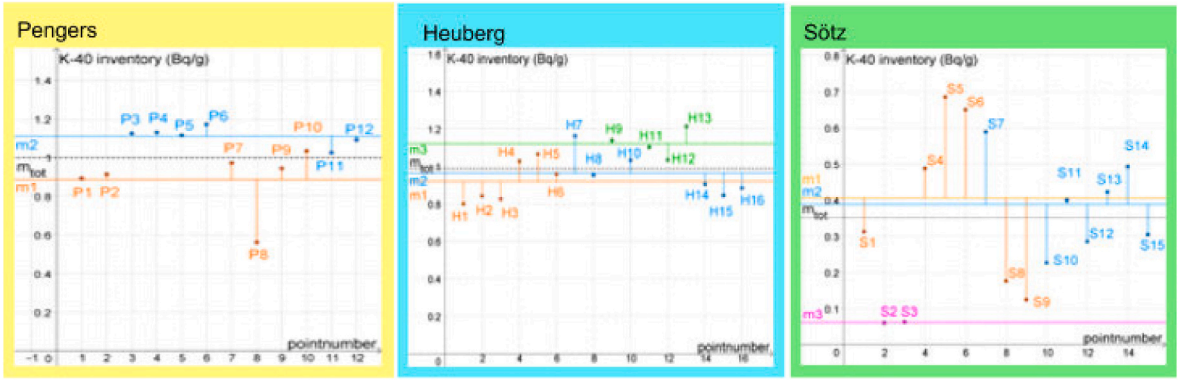

Fig. 13. Mass specific inventory of ^{40}K for Pengers, Heuberg and Sötz. Orange points represent meadow values, forest in blue, border area in green and gravel in pink. Horizontal line are associated mean values. Note: the scaling differs from figure to figure. (For interpretation of the references to colour in this figure legend, the reader is referred to the Web version of this article.)

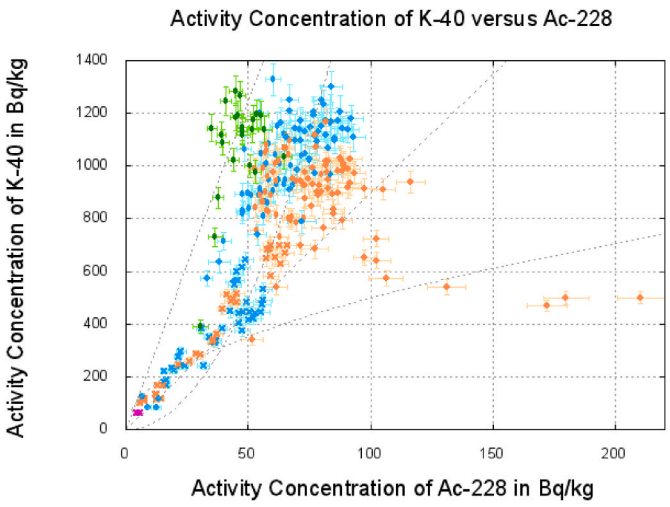

Fig. 14. Relation of activity concentration in Bq/kg - ^{40}K vs. ^{228}Ac (legend in Fig. 3 or as titles in Fig. 15).

these samples were on the same hill slope. In Heuberg, just like Pengers, no threshold for activity concentration (in Bq/m^3) was indicated.

In Sötz all activity concentrations (in Bq/kg) were below 70 Bq/kg and fell on average with increasing soil density. An approximation between gravel samples and S8 with high gravel percentage in lower levels was observed. Based on a silo building nearby, mechanical mixing in S9 is assumed. Activity concentrations (in Bq/m^3) showed ambivalent tendencies. Many courses remained decreasing.

Explained variances for the top soil layer were 51% (vol.) and 74% (mass) in Pengers, 69% (vol.) and 70% (mass) in Heuberg and 42% (vol.) and 49% (mass) in Sötz. Explained variances for inventories were 58% (vol.) and 20% (mass) in Pengers, 56% (vol.) and 65% (mass) in Heuberg and 34% (vol.) and 35% (mass) in Sötz (for mass inventories see Fig. 16 or the supplementary data file). The explained variance of the difference "A(i+1) – A(i)" of activity concentration (in Bq/m^3) of neighboring layers showed 62% explained variance for layer 3–4, where grass roots end, in Pengers, 5% in Heuberg and 9% in Sötz. The trend coincided with that of ^{40}K in most layers.

In literature radionuclides are compared to ^{232}Th because of its lower mobility (Blanco Rodríquez et al., 2012; Schulz, 1965 as cited in Nenadović et al., 2012).

The relation between ^{40}K and ^{228}Ac activity concentrations (in Bq/kg) were different on each site (Fig. 8). In Sötz a linear proportionality with a factor near 10 seems to fit. The other sites formed a rather unstructured point cloud. Although sites populated with conifers showed increased ^{40}K activity concentration (in Bq/kg) in comparison to other vegetation types. Manigandan and Chandar Shekar (2017) reported a relation between ^{40}K and ^{232}Th, which resembles a square-root function between ^{40}K in dependency on ^{228}Ac (see there for the exact exponent). In the present data only Sötz data with the Pengers spike could have such a curve shape ($y = 50 \bullet \sqrt{x}$ was plotted in Figs. 14 and 15). The sample of deforestation/young forest (H13) show high ^{40}K activity concentration (in Bq/kg), the recovering process seems to be completed fast (in contrast: *potassium recovers slowly after disturbances (clear-cutting)* in Fujiyoshi et al. (2014)).

In Fig. 14 (and 15) a spreading tendency between ^{228}Ac and ^{40}K depending on vegetation type is visible, which could be only partially explained by measurement uncertainties. For low activities the deviations from linearity were small. For greater values the activities of the sites appear to separate according to vegetation categorization and the path becomes quadratic ($y = 0.2 \bullet x^2$ was plotted). Most activity concentrations (in Bq/kg) lie between auxiliary lines $y_1 = 9$ x and $y_2 = 25$ x.

Manigandan and Chandar Shekar (2017) also suggested a nearly quadratic relation between ^{238}U in dependency on ^{232}Th (see there for the exact exponent). Besides Sötz forest and Pengers meadow this assumption could hold (Figs. 17–20). Sötz forest and Pengers meadow resemble an at least cubic (6th order polynomial matches the curvature)

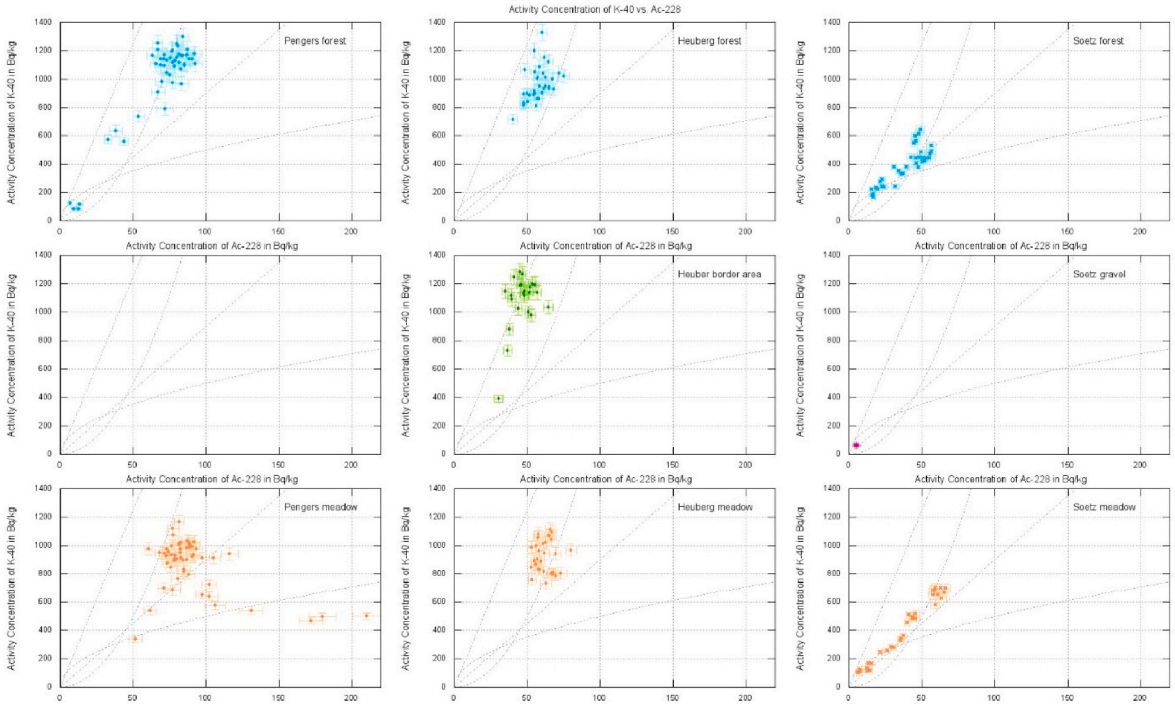

Fig. 15. Here the data points of Fig. 14 are split according to site location and vegetation category. Note: The central figure in the column for Pengers contains no data points. There are only two categories in Pengers.

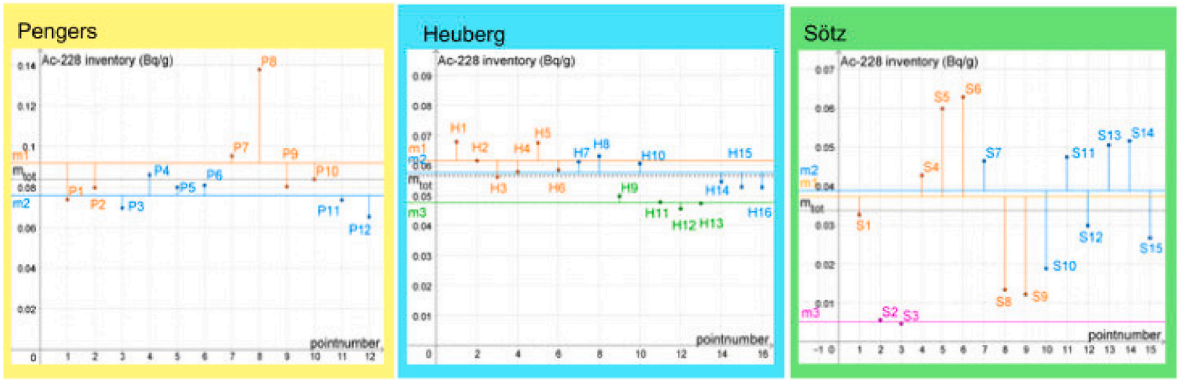

Fig. 16. Mass specific inventory of ^{228}Ac for Pengers, Heuberg and Sötz. Orange points represent meadow values, forest in blue, border area in green and gravel in pink. Horizontal line are associated mean values. Note: the scaling differs from figure to figure. (For interpretation of the references to colour in this figure legend, the reader is referred to the Web version of this article.)

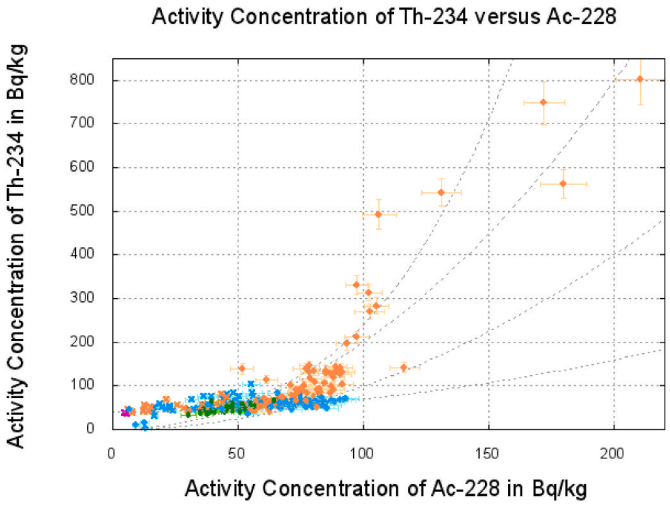

Fig. 17. Relation of activity concentration in Bq/kg - ^{234}Th vs. ^{228}Ac (legend in Fig. 3 or as titles in Fig. 18).

dependency between ^{234}Th and ^{228}Ac, which is of an even higher order between ^{214}Bi and ^{228}Ac in Sötz forest (Figs. 21 and 22). Auxiliary functions in Figs. 17–22 are $y = 0.01 \bullet x^2$, $y = 0.02 \bullet x^2$, $y = 40 + 0.003 \bullet x^2$ and $y = 40 + 0.0002 \bullet x^3$. The first layer depletion of ^{40}K in $P5_1$, $P11_1$ and $P12_1$ is unresolved (most likely induced by conifer litter, but not in the other forest samples).Vukašinović et al. (2018) assumed that ^{226}Ra became partially cycled by trees, while ^{232}Th remained part of the soil. Therefore a depletion of ^{224}Bi in the first layer as typical for (coniferous) forest vegetation as in Pengers may be assumed due to (conifer) litter fall. An enrichment in the third layer as in Heuberg H16 and Sötz S12 (and S11) could be influenced by water, by extensive litter fall – these sites (H16, S11 and S12) were covered with dead tree trunks – and in Sötz by cellular dolomite.

3.7. Ternary diagrams

Ternary diagrams are usually used in chemistry and geology. Additionally, they have been applied for the representation of a secular disequilibrium of a radioactive series or for comparing radionuclides of different radioactive series (Rosholt, 1983; Andretta et al., 1992; Bhattacharya et al., 2018; Erbek and Dolmaz, 2018; Kaniu et al., 2018; Bezuidenhout, 2020). Ternary diagrams based on log-ratio have also been used for the analysis of compositional data based on Aitchison geometry (Buccianti et al., 2006). Here a calculation via barycentric coordinates is used, because a statistical evaluation only for correction factors is considered. The advantage is to link all three values in each coordinate of the point in the ternary diagram.

3.7.1. Theory on ternary equilibrium diagrams

In literature, ratios between different parent and daughter radionuclides have been investigated frequently (for many: Vukašinović et al., 2018). Ternary diagrams for $^{238}U^e$ - $^{226}Ra^e$ - ^{210}Pb provide the opportunity to observe the equilibrium status for these three radionuclides at the same time (distance to the center point) as well as for two radionuclides (distance to median line). The representation is trivially invariant with respect to the units of activity concentration in Bq/mass or Bq/volume for layer values. The invariance for inventories will hold, if the density of the radiologically measured layer sample is the same as the density of the total layer sample.

Both ratios and ternary equilibrium diagrams lack providing the value of measured activities, but make different sites with different settings comparable.

3.7.2. Application of ternary equilibrium diagrams

In Fig. 3 calculated “equilibrium points” for the mass-specific inventory have been joined together as polygons for each site to focus on the site according to vegetation category. Here data at hand from the (traffic exposed) Krauthügel (in Salzburg-City, data from RMLS) and Alpine pastures (in Salzburg-County, data from Meusburger et al., submitted) have been added. Single points could be observed in the following figure (Fig. 4).

The polygon of Heuberg meadow lies within the polygon of Heuberg forest and the polygon of Heuberg border area resembles a polygon line nearer to the point of equilibrium.

The wide range of disequilibria is striking. Alpine pasture data show a shift to ^{210}Pb because of aeolian deposition and a shift to ^{238}U. Alpine pasture regions often lack organic material in (deeper layers of) soil. Vukašinović et al. (2018) has found small $^{238}U/^{226}$Ra ratios in the topsoil. She assumed a^{226}Ra enrichment there and took the abundant SOM (soil organic matter) content into account. A strong radium retention in organic material in soils is assumed because of a negative correlation between $^{238}U/^{226}$Ra and SOM content by other authors (Vandenhove, 2009 as cited in Vukašinović et al., 2018). According to Thørring et al. (2020) element-dependent differences in soil chemical behavior (Ahmad et al., 2019), mobility, plant uptake (vertical distribution), bioturbation and redistribution of mineral due to drainage from nearby areas can cause site specific deviations (of ^{226}Ra). Blanco Rodríquez et al. (2012) suggested a cause of a disequilibrium in surface layers to be ^{222}Rn gas emission and subsequent surface deposition of ^{210}Pb (Sheppard, 2008 as cited in Thørring et al., 2020; Charro et al., 2013). In a region of hot springs in south east Europe a disequilibrium between ^{238}U and ^{226}Ra was found, indicating the addition of ^{226}Ra by

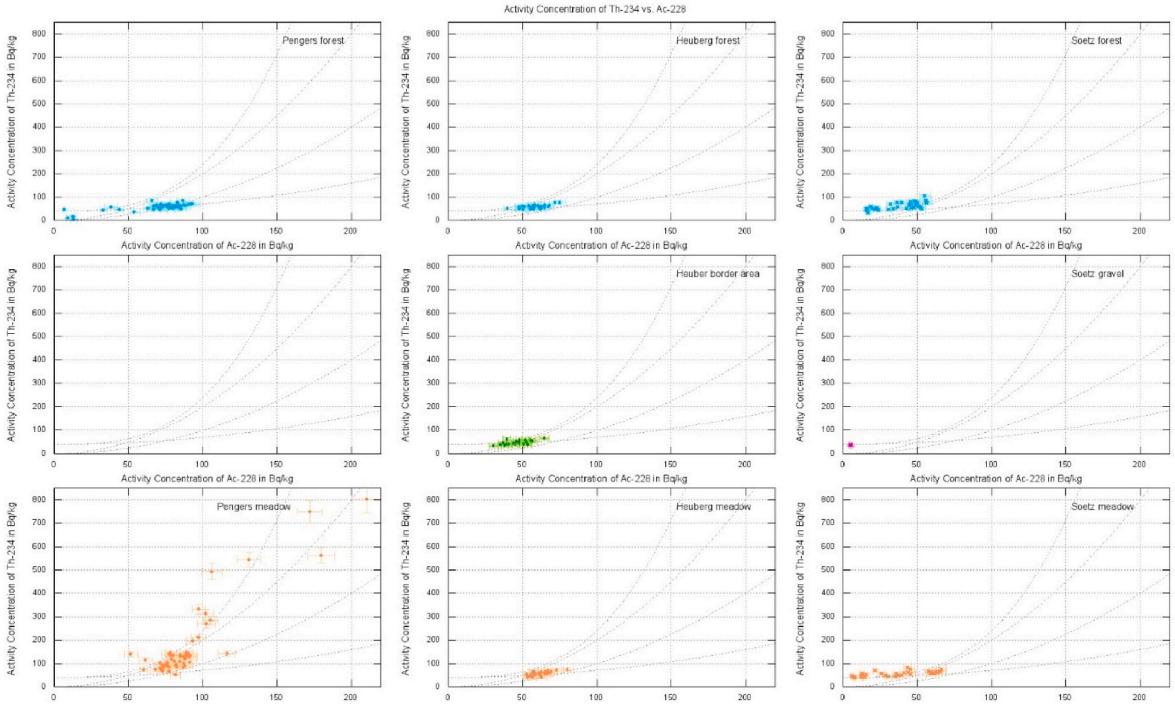

Fig. 18. Here the data points of Fig. 17 are split according to site location and vegetation category. Note: The central figure in the column for Pengers contains no data points. There are only two categories in Pengers.

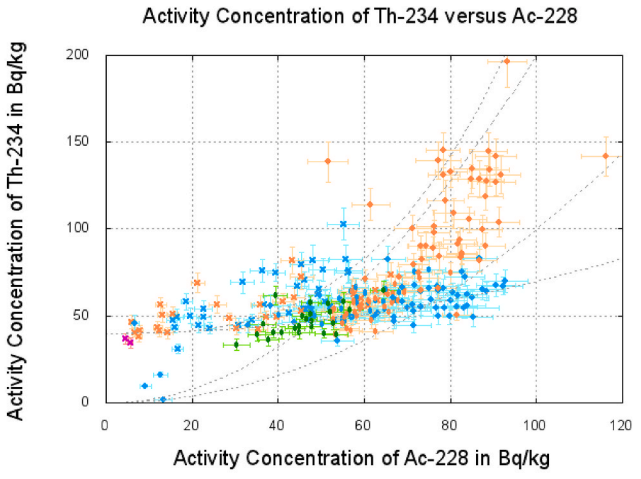

Fig. 19. Relation of activity concentration in Bq/kg - ^{234}Th vs. ^{228}Ac – detail (legend in Fig. 3 or as titles in Fig. 20).

spring water (Padovani et al., 2018). Charro et al. (2013) also observed a lower average concentration of ^{238}U than ^{226}Ra. According to this behavior, a shift to the right vertex (^{226}Ra^{e}) in ternary equilibrium diagrams can be identified. In Pengers and Sötz most ternary equilibrium diagram points of meadows are clearly separated from points of forest samples (except S4 and P10). Uncultivated Heuberg meadows do not show such separation, but Heuberg border area does.

In topsoil a disequilibrium in the radioactive series of ^{238}U has often been examined (Kekelidze et al., 2017; surface depletion: Navas et al., 2011). The equilibrium is disturbed by selective leaching due to different mobility of daughter and parent radionuclides in soil/water and by anthropogenic influence. In a comparison between U and radium, U is more mobile than radium due to leaching uranyl complexes (Koch, Steindl and Pröhl, 2001, as cited in Vukašinović et al., 2018; (slight depletion of ^{226}Ra) Tagami and Uchida, 2009, as cited in Charro et al., 2013; Harmsen and de Haan, 1980). The higher situated part of the sample region in Sötz is part of the Opponitz formation with cellular dolomite (containing $RaSO_4$) (Pleiderer et al., 2002: Fig. 2: geological general map). This could intensify radium immobility compared to U.

In literature ^{210}Pb is observed in comparison to ^{226}Ra, the difference is called ^{210}Pb$_{exc}$ (excess lead) or in comparison to ^{238}U then denoted ^{210}Pb$_{neq}$ (not equilibrium lead). In case of equilibrium each ratio of parent and daughter radionuclide should be equal to one, but they seldom are. Different accumulation distributions occur due to (wet or dry) deposition events (originated in the combustion of fossil fuels or decay products of ^{222}Rn) such as canopy and runoff effects (Fujiyoshi and Sawamura, 2004; Thørring et al., 2020; Scarciglia et al., 2020). Fujiyoshi and Sawamura (2004) found elevated values of ^{210}Pb down to a depth of 10 cm in forest soils. ^{210}Pb$_{exc}$ decreases with increasing depth; therefore, ^{210}Pb reaches equilibrium in lower layers (Scarciglia et al., 2020). Scarciglia et al. (2020) reported, *a lack of vegetation cover coincides with values near equilibrium for ^{210}Pb* (in cultivated or abandoned fields), *as well as a* (plant caused) *higher concentration of ^{210}Pb are observed in soil profiles in forests* (Scarciglia et al., 2020). Thørring et al. (2020) observed a decreasing trend for ^{210}Pb in two plant species with increasing soil levels. He found higher concentration in old grass leaves due to different growth rate or longer accumulation period, which may influence remote sensing.

The average ratios of ^{210}Pb to ^{226}Ra for all layers are 0.79/0.83/0.83 for meadows and 3.22/0.93/0.60 for forests in Pengers/Heuberg/Sötz. The obtained ratios of these sites are mainly consistent with reported ratios ^{210}Pb/^{226}Ra in the literature (0.7–1.36 in Vukašinović et al., 2018; up to 2.0 in Anagnostakis (2011 as cited in Vukašinović et al., 2018); up to 8.73 in Kekelidze et al., 2017; up to 2–3 in Thørring et al., 2020). The values of the layers show greater deviations from these values.

An observation of a sequence of ternary equilibrium diagrams for 4 different layers (Figs. 6–9) show increased ^{210}Pb activity in the top soil layers and a decreasing tendency with depth. The layer reaching equilibrium depends on the location. On alpine pastures equilibrium is reached in greater depths than for example in the mid-town test-site of Krauthügel in Salzburg ^{210}Pb$_{exc}$ data disappeared in a depth of 20 cm.

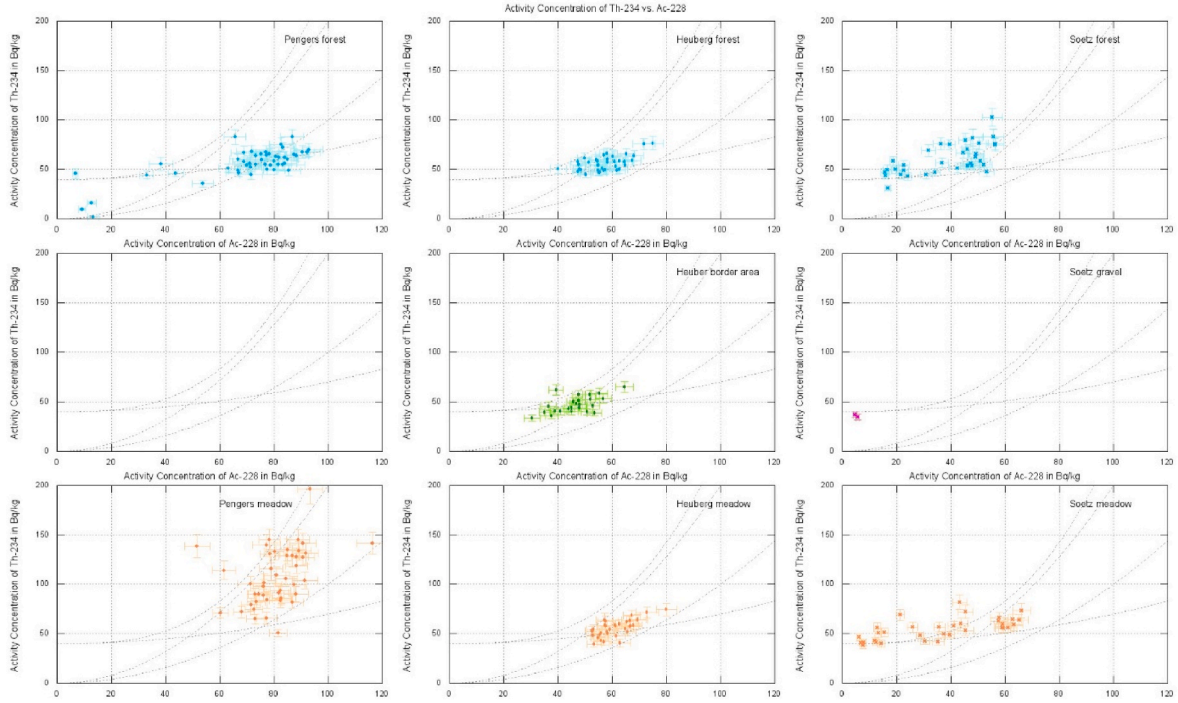

Fig. 20. Here the data points of Fig. 19 are split according to site location and vegetation category. Note: The central figure in the column for Pengers contains no data points. There are only two categories in Pengers.

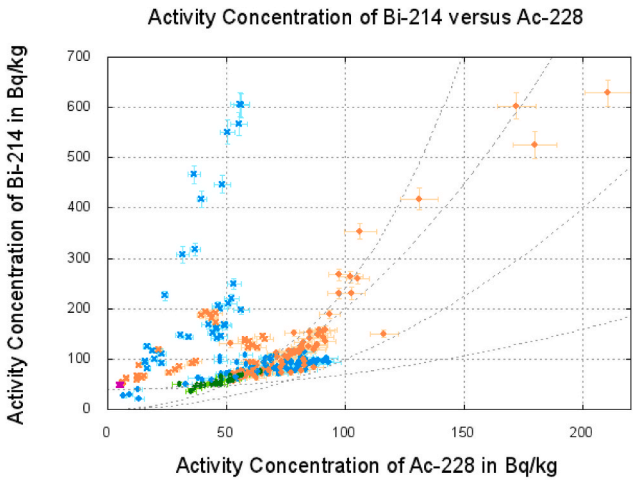

Fig. 21. Relation of activity concentration in Bq/kg - ^{214}Bi vs. ^{228}Ac (legend in Fig. 3 or as titles in Fig. 22).

Pengers, Heuberg und Sötz data go along with Fujiyoshi and Sawamura (2004) observations. Extraordinary high ^{226}Ra activity in each layer is found in Sötz forest, especially at a depth of 10–15 cm in S11 and S12, besides a small shift to ^{226}Ra abundance in most samples.

3.7.3. Ternary adjustment diagram – an example

Here ternary diagrams with the radionuclides ^{238}U^{e2}, ^{232}Th^{e} and ^{40}K are called ternary "adjustment" diagrams. These radionuclides will be detected in an aero-gamma-spectrometric measurement. A comparison between the vectors consisting of different radionuclides' activities and/or points in a ternary adjustment diagram of the surface exploration and the soil samples will disclose each eminent discriminative environmental influence on elementwise sensing. The mathematical theory is given in Appendix B; here, only an application is shown. For example assume a activity concentration (in Bq/kg) by remote sensing of 48.9 Bq/kg for ^{238}U^{e2} via ^{214}Bi, of 14.80 Bq/kg for ^{232}Th^{e} and of 119.69 Bq/kg for ^{40}K - these will be referenced by the remote data vector $y = (48.9, 14.8, 199.69)^T$ - contrasted by a mass-specific inventory in a soil sample of 188.62 Bq/kg for ^{238}U^{e2} via ^{214}Bi, 42.70 Bq/kg for ^{232}Th^{e} and 487.94 Bq/kg for ^{40}K. It will be referenced by reference vector $x = (188.62, 42.7, 487.94)^T$. These two vectors are needed for calculation of the adjustment vector $z_0 = \alpha_x \bullet x$ with $\alpha_x = \frac{\langle y|x\rangle}{\langle x|x\rangle}$ ($\langle .|. \rangle$ denotes the Euclidean scalar product in $\mathbb{R}^3$). This is derived in lemma 4 in the theory section in Appendix B. Then the adjustment vector z_0 has minimal distance to the remote data vector y and will coincide with the reference point of the soil sample in the ternary diagram.

Here, an adjustment factor of $\alpha_x \sim 0.2478$ can be calculated and therefore z_0 will consist of ^{238}U^{e2}: 46.73 Bq/kg, ^{232}Th^{e}: 10.57 Bq/kg and ^{4} K: 120.90 Bq/kg. Then elementwise correction factors $\frac{y_i}{z_{0i}}$, $1 \le i \le 3$, can be calculated, which in this case were ~1.04 for ^{238}U^{e2}, ~1.4 for ^{232}Th^{e} and ~0.99 for ^{4} K. A correction factor lower than one could be interpreted in the sense that the remote sensed value should have been greater, implying additional dampening. A correction factor above one may be interpreted as the remote sensing measured additional sources not originated in the soil. In this case more ^{232}Th^{e} sources are "non-soil" than of ^{238}U^{e2}. Unfortunately at this moment not enough or suitable data from remote sensing are available for an analysis according to vegetation type.

4. Summary and conclusion

The first objective was a statistical identification of distinctions between soil samples from meadows and forests, where a categorization between coniferous and deciduous forest was considered. The border area in Heuberg with more conifers showed deviations to other categories. In Heuberg distinctions between meadows and beech forests, the dominating deciduous tree species, were rare. In Sötz in particular geological and mineralogical characteristics dominated the absolute level of activities at the sites. Very local differences often evolve from topography, climate and human influence as shown by the assumed

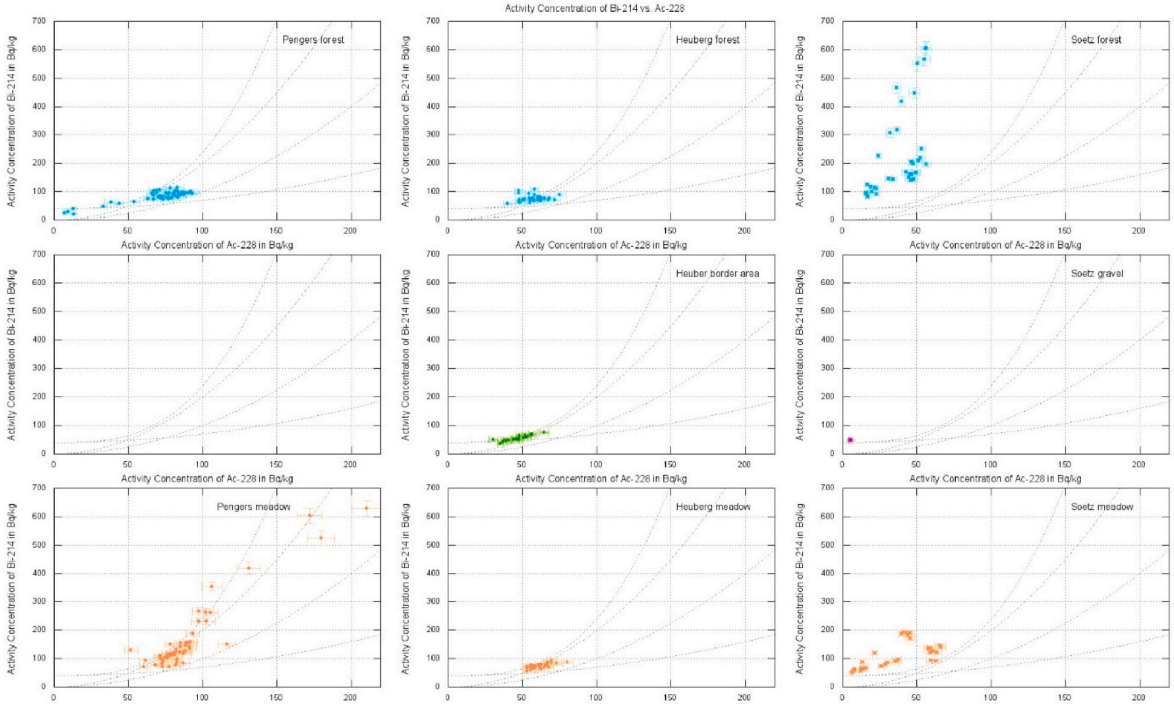

Fig. 22. Here the data points of Fig. 21 are split according to site location and vegetation category. Note: The central figure in the column for Pengers contains no data points. There are only two categories in Pengers.

hydromorphic soil in Pengers meadow. Fertilized meadows imply higher activities of ^{238}U, ^{232}Th and ^{40}K. Topsoil densities were often influenced by slope in association with vegetation type implying different SOM contents.

The kind of secular disequilibrium is different in meadows and forests. In ternary equilibrium diagrams for inventories meadows are more likely to occupy points to the left edge (less ^{226}Ra) in contrast to the points of forest samples of the same site. This could be a consequence of vegetation density or homogeneity of this density because uncultivated meadow samples in Heuberg occupy the same region in ternary equilibrium diagram as forest samples. Samples with more coniferous trees nearby are supposed to show less ^{226}Ra than samples from deciduous forests.

The aeolian deposited radionuclide ^{210}Pb decreases exponentially with soil density. Vegetation density effects interception and the amount of all aeolian deposited radionuclides. Differences in the deposition rates seem to depend on the vegetation period influencing deposition probability and the kind of litter fall.

Topsoil layers are extremely exposed to exogenous processes which could significantly influence results of remote sensing.

- In forest samples topsoil densities are usually low but increase faster than meadow density. The variability is higher than in meadow samples.
- Layer 1 and 2 show eminent differences in ^{234}Th activity regarding vegetation type. Those samples located in a border area between meadow and forest in Heuberg show lower ^{234}Th inventories of both types than average in Heuberg.
- In Sötz radium-226 concentration was increased, most likely either a local effect of the cellular dolomite in the Opponitz formation which causes an accumulation as $RaSO_4$ or the influence of moisture. Based on the presentation in ternary equilibrium diagrams ^{226}Ra should be more effected by the type of vegetation due to kind of litter fall, biological activity (CO_2) and/or repeated cycling of dead wood from dead twigs or trunks.
- ^{210}Pb activities are mostly elevated in topsoil layers with a steeper decrease in forests soil layer 1 to 2.
- Increase of thorium equivalent (^{228}Ac) activity from layer 1 to 2 is greater in forest than in meadow. This means increase in forest is paired with constant values in meadow like in Pengers or constant values in forest are paired with decrease in meadows like in Heuberg. Sötz varies locally on a smaller scale regarding a lack of thorium in the parent rock.
- ^{40}K activities are often reduced in the topsoil layer, more in Heuberg border area, except all samples in Sötz. But Heuberg ^{40}K activities are less reduced compared to the reduction of ^{214}Bi or ^{228}Ac in first to second layer. The increase from layer 1 to 2 seem to be steeper with coniferous trees around. When the parent rock is not K-bearing, the depth distribution varies significantly depending on other local constituents (SOM, fertilization, local topography). Vegetation influences such local setting in Sötz only to a small extent.

Declaration of competing interest

The authors declare that they have no known competing financial interests or personal relationships that could have appeared to influence the work reported in this paper.

Data availability

Data will be made available on request.

Acknowledgements

This work is primarily supported by the Geological Survey of Austria (Geologische Bundesanstalt, GBA) – as part of the VEGAM project: Multidisciplinary study to determine accurate vegetation and topography corrections for airborne gamma-ray spectrometry using an UAV measuring system.

Appendix D. Supplementary data

Supplementary data to this article can be found online at https://doi.org/10.1016/j.jenvrad.2022.107038.

Appendix A. Explained Variance – Formula

For each category k with a number of samples denoted with n_k the formula

$$\sum_k \sum_{i=1}^{n_k} (x_{ki} - \overline{x})^2 = \sum_k \sum_{i=1}^{n_k} (x_{ki} - \overline{x_k})^2 + \sum_k n_k \bullet (\overline{x_k} - \overline{x})^2 \tag{A.1}$$

holds. Where x_{ki} denoted the ith sample in category k, $\overline{x_k}$ the mean value in category k and $\overline{x}$ the mean value for all samples of all categories. The term on the left side is usually denoted as total square sum and the first term on the right side of the equation is denoted as effect square sum.

Then the explained variance is defined as ratio between effect square sum and total square sum.

For more details see for example Dormann (2017).

Appendix B. Mathematical Theory on an Algorithm using Ternary Adjustment Diagrams

Let be A(0|0), B(1|0) and $C\left(\frac{1}{2}\middle|\frac{\sqrt{3}}{2}\right)$ the coordinates of the vertices of the ternary adjustment diagram.

Let be x_A the activity concentration of ^{238}U, x_B the (specific) activity of ^{232}Th and x_C that of ^{40}K from the soil samples, forming the reference-vector. Name y_A, y_B und y_C the corresponding activity concentrations acquired from the surface measurement forming the remote data vector. Then let the vectors be $x = (x_A \quad x_B \quad x_C)^T$ und $y = (y_A \quad y_B \quad y_C)^T$.

Let furthermore κ_1 denote $\kappa_1 = x_A + x_B + x_C$, as well as $\kappa_2 = y_A + y_B + y_C$ and $\kappa = \kappa_1 \bullet \kappa_2$.

Also, $w_i = \begin{pmatrix} x_i \\ y_i \end{pmatrix}$ with $i \in \{A, B, C\}$. With these declarations the operation $\bigotimes$ is defined as follows:

$$(w_A + w_C) \bigotimes w_B := (x_A + x_C) \bullet y_B - (y_A + y_C) \bullet x_B$$

The reference point $S_x = \frac{x_A \bullet A + x_B \bullet B + x_C \bullet C}{x_A + x_B + x_C}$ of the soil sample and the remote data point $S_y = \frac{y_A \bullet A + y_B \bullet B + y_C \bullet C}{y_A + y_B + y_C}$ of the surface measurement in the ternary adjustment diagram differ by the vector $\vec{S_x S_y}$ in the ternary diagram, where

$$\vec{S_x S_y} = \frac{1}{\kappa} \bullet \{(w_B + w_c) \bigotimes w_A \bullet A + (w_A + w_c) \bigotimes w_B \bullet B + (w_A + w_B) \bigotimes w_C \bullet C\}$$

Under optimal measuring conditions the vector $\vec{S_x S_y}$ is the null vector.

Lemma 1a. *If and only if the activities of the soil samples and the activities of the surface measurement are proportional with the same factor for all three radionuclides, then their points in a ternary diagram will coincide.*

Proof: *One direction of the proof is a simple calculation with factorization. The second direction of the lemma results from* lemma 1b *and an invariance of the scheme for rotation of vertex-declaration.* ✓

Lemma 1b. *The given set of linear equations* (*originating in coordinates of* $\vec{S_x S_y} = \vec{0}$)

$$I.\ \frac{x_B + x_C}{x_A} = \frac{z_B + z_C}{z_A}$$

$$II.\ \frac{x_A + x_C}{x_B} = \frac{z_A + z_C}{z_B}$$

$$III.\ \frac{x_A + x_B}{x_C} = \frac{z_A + z_B}{z_C}$$

have a single-parameter solution:

$$\begin{pmatrix} z_A \\ z_B \\ z_c \end{pmatrix} = k \bullet \begin{pmatrix} x_A \\ x_B \\ x_C \end{pmatrix} = [x], k \in \mathbb{R}$$

Proof: *This is easily calculated.*

There is no other kind of activity-vector to occupy the same point in a ternary adjustment diagram.

Lemma 2. *If* $k_3^x := \frac{x_A + x_B}{x_C} = \frac{y_A + y_B}{y_C} =: k_3^y$ *and* $k_2^x := \frac{x_A + x_C}{x_B} = \frac{y_A + y_C}{y_B} =: k_2^y$ *hold, then the adjustment points* S_1 *und* S_2 *have the same coordinates in the ternary adjustment diagram and the translations vector is the zero vector.*

Proof: *This is implied by the ansatz* A=(0|0) *and lemma* 1.

A match of the activities of the soil sample and of the surface measurement cannot be expected, but the necessary corrections could be calculated from ternary adjustment diagrams.

The equations of lemma 1 *can be used for a constructing iteration of a suitable adjustment vector beginning with* $y_A^{(0)} = y_A$ *and the iteration*

$$\frac{y_A^{(n+1)}}{y_B^{(n)} + y_C^{(n)}} = \frac{x_A}{x_B + x_C}$$

in the form of

$$y_A^{(n+1)} = \frac{x_A}{x_B + x_C} \bullet \left(y_B^{(n)} + y_C^{(n)} \right).$$

Analog iterations for the other radionuclides evolved to a tangled three-dimensional iteration with the following matrix T. *Here* $\|x\|_2$ *denotes the Euclidean norm of* x.

Lemma 3. Let $a = \frac{x_A}{x_B + x_C}$, $b = \frac{x_B}{x_A + x_C}$ and $c = \frac{x_C}{x_A + x_B}$ as well as the matrix $T = \begin{pmatrix} 0 & a & a \\ b & 0 & b \\ c & c & 0 \end{pmatrix}$

Then the greatest eigenvalue of the matrix T is $\lambda_1 = 1$ with the associated eigenvector $v_1 = \frac{x}{\|x\|_2}$.

Also hold: $-\frac{1}{2} \le \lambda_2 < 0$ and $-1 < \lambda_3 \le -\frac{1}{2}$

and with $[x]$ as linear span

$$\lim_{n \to \infty} (T^n \bullet y) = \lim_{n \to \infty} y^{(n)} \in [x]$$

Proof:

The characteristic polynomial of the matrix T has root 1. This can easily be checked. Polynomial long division leads to a quadratic equation with the solutions: $\lambda_{2,3} = \frac{1}{2} \bullet (-1 \pm \sqrt{1 - 8 \bullet a \bullet b \bullet c})$. The discriminant is smaller than one, if all measured activity conccentrations (in Bq/kg) are greater than the detection limit, therefore $a, b, c > 0$.

The solutions are real because $a \bullet b \bullet c \le \frac{1}{8}$ holds. The greatest value $\frac{1}{8}$ evolves, if $a = b = c = \frac{1}{2}$. The Hessian matrix of T itself is negative semi-definite with an infinite number of maxima ([.]).

Let be $y = \sum_{i=1}^{3} \alpha_{y,i} \bullet v_i$, where $v_i, 1 \le i \le 3,$ denote the eigenvectors of T

$$T^n \bullet y = T^n \bullet \sum_{i=1}^{3} \alpha_{y,i} \bullet v_i = \sum_{i=1}^{3} \alpha_{y,i} \bullet T^n \bullet v_i = \sum_{i=1}^{3} \alpha_{y,i} \bullet \lambda_i^n \bullet v_i \underset{n \to \infty}{\longrightarrow} \alpha_{y,1} \bullet v_1 = \alpha_{y,1} \bullet \frac{x}{\|x\|_2} \in [x]$$

All shares not belonging to the first eigenvector will be diminished in an iteration.

This algorithm converges numerically (in Excel) only for special vectors x, possibly due to a number precision that is too low. In many cases the result lies in the linear span of x. In case of convergence a minimum in the Euclidian norm arise, which can be calculated directly.

Lemma 4. *Let be* $\alpha = \frac{\langle y|x \rangle}{\sqrt{\langle x|x \rangle}} = \langle y|v_1 \rangle$ *and* $z_0 = \alpha \bullet v_1$.

Then the reference point of x *and the adjustment point of* z_0 *coincide in the ternary adjustment diagram and* $\|y - z\|_2$ *is minimal for* $z = z_0$ *for all* z *in the linear span of* x.

Proof:

The first part of lemma 4 *is proven by lemma* 1 *a.*

For the second part let be $z = \alpha_{z,1} \bullet v_1$ *and* $y = \sum_{i=1}^{3} \alpha_{y,i} \bullet v_i$, *where* $v_i, 1 \le i \le 3,$ *denote the eigenvectors of* T. *Then*

$$\|y - z\|_2^2 = \left\| \left(\alpha_{y,1} - \alpha_{z,1} \right) \bullet v_1 + \alpha_{y,2} \bullet v_2 + \alpha_{y,3} \bullet v_3 \right\|_2^2 = \langle y - z | y - z \rangle = \left(\alpha_{y,1} - \alpha_{z,1} \right)^2 + \alpha_{y,2}^2 + \alpha_{y,3}^2$$

is minimal, if $\alpha_{z,1} = \alpha_{y,1}$.

Corollary

In other words a vector of activities – adjustment vector – can be calculated, which inherits the same position in a ternary diagram as the reference vector (the activity vector of the soil sample) with a minimal (Euclidean) distance to the remote data vector (the activity vector of the surface measurement). The coordinate wise ratio of the adjustment vector and the activity vector of the surface measurement $cf_i = \frac{y_i}{z_{0i}}$, $i \in \{A, B, C\},$ *can be used as correction factors. A correction factor of cf lower than one implies that the surface measurement was too low. Between source and detector signals were lost. A correction factor of cf above one implies that the surface measurement was too high. Between source and detector signals were added.*

Sometimes it is inconvenient applying normalized eigenvectors, in that case $z_0 = \alpha_x \bullet x$ *and* $\alpha_x = \frac{\alpha}{\|x\|_2} = \frac{\langle y|x \rangle}{\langle x|x \rangle}$ *can be used.*

A functional analytical assessment of ternary adjustment diagrams comprises projection theory (in Meise and Vogt, 1992; *for example). The linear mapping* $T = \lim_{n \to \infty} T^n$ *projects Euclidean* $\mathbb{R}^3$ *orthogonal onto a one-dimensional linear subspace.* Lemma 4 *is an application of unique minimizing the share in orthogonal space (distance).*

It also can be seen as minimizing problem for the distance to y *under the condition occupying the same location as* x *in a ternary diagram.*

Appendix C. *Inventories – Formulas*

Volume specific inventory

$$\overline{I_{Vk}} = \frac{1}{V_k} \bullet \sum_{i=1}^{n_k} A_{Vki} \bullet V_{k,i}$$

Mass specific inventory

$$\overline{I_{mk}} = \frac{1}{m_k} \bullet \sum_{i=1}^{n_k} A_{mki} \bullet m_{k,i}$$

Area specific inventory for radiocesium

$$I_k = \frac{d_k}{V_k} \bullet \sum_{i=1}^{n_k} A_{Vki} \bullet V_{k,i}$$

I_k	*Total inventory for ^{137}Cs (Bq/cm^2) in sample point k*	$\overline{I_{Vk}}, \overline{I_{mk}}$	*Average inventory (Bq/cm^3, resp. Bq/g) in sample point k*
A_{mki}	*Activity concentration in Bq/g in the i^{th} layer of sample point k*	A_{Vki}	*Activity concentration in Bq/cm^3 in the i^{th} layer of sample point k*
Relation of both layer activities:		$A_{Vki} = A_{mki} \bullet \frac{m_{mess,k,i}}{V_{mess,k,i}}$	
Further Denotations			
$m_{k,i}$	*Mass of the total sample of the i^{th} layer in sample point k*	$m_{mess,k,i}$	*Mass of the radiologically measured sample of the i^{th} layer in sample point k*
$V_{k,i}$	*Volume of the total sample of the i^{th} layer in sample point k*	$V_{mess,k,i}$	*Volume of the radiologically measured sample of the i^{th} layer in sample point k*
		n_k	*Number of layers in sample point k*
$d_{k,i}$	*thickness of the i^{th} layer in sample point k*	$d_k = \sum_{i=1}^{n_k} d_{k,i}$	*Core length of sample point k*
		$m_k = \sum_{i=1}^{n_k} m_{k,i}$	*Total mass of the core in sample point k*
		$V_k = \sum_{i=1}^{n_k} V_{k,i}$	*total volume of the core in sample point k*

References

Ahmad, A.Y., Al-Ghouti, M.A., AlSadig, I., Abu-Dieyeh, M., 2019. Vertical distribution and radiological risk assessment of ^{137}Cs and natural radionuclides in soil samples. Nature Research Scientific Reports 9, 12196. https://doi.org/10.1038/s41598-019-48500-x.

Ahmed, H., Young, S.D., Shaw, G., 2014. Factors affecting uranium and thorium fractionation and profile distribution in contrasting arable and woodland soils. J. Geochem. Explor. 145, 98–105.

Andretta, D., Voltaggio, M., Taddeucci, A., Polizzano, C., 1992. Disequilibrium of uranium, thorium and radium isotopes in pliocenic clays. Radiochim. Acta 58/59, 415–421.

Bhattacharya, T., Madhavi Shankar, V., Ram Mohan Reddy, B., Thangavel, S., Sharma, P. K., 2018. Radioactivity levels in the atomic mineral occurrence along dharmapuri shear zone in parts of vellore, krishnagiri, dharmapuri and Salem districts of Tamil Nadu,India. Appl. Radiat. Isot. 132, 135–141. https://doi.org/10.1016/j.apradiso.2017.11.028.

Berka, R., Katzelberger, Ch, Philippitsch, R., Schubert, G., Korner, M., Landstetter, C., Motschka, K., Pirkl, H., Grath, J., Draxler, A., Hörhan, Th, 2014. Erläuterungen zur geologischen Themenkarte Radionuklide in den Grundwassern, Gesteinen und Bachsedimenten Österreichs 1:500.000. Geologische Bundesanstalt, Wien.

Bezuidenhout, J., 2020. The investigation of natural radionuclides as tracers for monitoring sediment processes. J. Appl. Geophys. 181, 104135 https://doi.org/10.1016/j.jappgeo.2020.104135.

Blanco Rodríquez, B.P., Vera Tomé, F., Lozano, J.C., 2012. Vertical distribution of natural radionuclides in soils. EPJ Web Conf. 24, 05001 https://doi.org/10.1051/epjconf/20122405001.

Buccianti, A., Mateu-Figueras, G., Pawlowsky-Glahn, V. (Eds.), 2006. Compositional Data Analysis in Geosciences: from Theory to Practice. Geological Society, London, Special Publications, p. 264.

Charro, E., Pardo, R., Peña, V., 2013. Chemometric interpretation of vertical profiles of radionuclides in soils near a Spanish coal-fired power plant. Chemosphere 90, 488–496. http://dx.doi.org/10.1016/j.chemosphere.2012.08.008.

Dormann, C., 2017. Parametrische Statistik[2]. Springer.

eBOD2 - Digitale Bodenkarte, https://bodenkarte.at/#/center/15.1611,48.8854/zoom/15.8, request from 30th June 2020, 2020.

Erbek, E., Dolmaz, M.N., 2018. In situ measurements of radionuclide concentrations in south of Mulga city, Turkey. Environ. Earth Sci. 77, 377. https://doi.org/10.1007/s12665-018-7562-8.

Fujiyoshi, R., Sawamura, S., 2004. Mesoscale variability of vertical profiles of environmental radionuclides (^{40}K, ^{226}Ra, ^{210}Pb and ^{137}Cs) in temperate forest soils in Germany. Sci. Total Environ. 320, 177–188. https://doi.org/10.1016/j.scitotenv.2003.08.007.

Fujiyoshi, R., Takekoshi, N., Okamoto, K., 2014. Variability of ^{40}K isotopic composition in forest soils under different environmental conditions. J. Radioanal. Nucl. Chem. 299, 1365–1371. https://doi.org/10.1007/s10967-013-2797-z.

Gueniot, B., Munier-Lamy, C., Berthelin, J., 1988. Geochemical behavior of uranium in soils, Part II. Distribution of uranium in hydromorphic soils and soil sequences for Surficial prospecting. J. Geochem. Explor. 31, 39–55.

Harmsen, K., de Haan, F.A.M., 1980. Occurrence and behaviour of uranium and thorium in soil in water. Neth. J. Agric. Sci. 28, 40–62.

He, Q., Walling, D.E., 1997. The distribution of fallout ^{137}Cs and ^{210}Pb in undisturbed and cultivated soils. Appl. Radiat. Isot. 48 (5), 677–690.

IAEA TECDOC 1363, 2003. Guidelines for Radioelement Mapping Using Gamma Ray Spectrometry Data. – International Atomic Energy Agency (IAEA), Nuclear Fuel Cycle and Materials Section, Austria.

Kaniu, M.I., Angeyo, K.H., Darby, I.G., 2018. Occurrence and multivariate exploratory analysis of the natural radioactivity anomaly in the south coastal region of Kenya. Radiat. Phys. Chem. 146, 34–41. https://doi.org/10.1016/j.radphyschem.2018.01.009.

Kekelidze, N., Jakhutashvili, T., Tutberidze, B., Tulashvili, E., Akhalkatsishvili, M., Mtsariashvili, L., 2017. Radioactivity of soils in Metskheta-Mtianeti region (Georgia). Annals of Agrarian Science 15, 304–311. https://doi.org/10.1016/j.aasci.2017.07.003.

Manigandan, P.K., Chandar Shekar, B., 2017. Soil depth profiles and radiological assessment of natural radionuclides in forest ecosystem. Radiochim. Acta 105 (6), 505–512. https://doi.org/10.1515/ract-2016-2662.

Meise, R., Vogt, D., 1992. Einführung in die Funktionalanalysis. vieweg studium, ISBN 3-528-07262-8.

Meusburger, T., Lettner H., Hubmer A. (submitted to Journal of Environmental Radioactivity). Effective Half-Lives for ^{137}Cs in Dairy Milk from Alpine Ecosystems and Their Controlling Factors.

Minty, B.R.S., 1997. Fundamentals of airborne gamma-ray spectrometry. AGSO J. Aust. Geol. Geophys. 17 (2), 39–50. Australia.

MortVedt J.J. (1994) Plant and soil relationships of uranium and thorium decay series radionuclides - a review. J. Environ Qual 23: 643 - 650.

Navas, A., Gaspar, L., López-Vicente, M., Machín, J., 2011. Spatial distribution of natural and artificial radionuclides at the catchment scale (South Central Pyrenees). Radiat. Meas. 46, 261–269. https://doi.org/10.1016/j.radmeas.2010.11.008.

Nenadović, S., Nenadović, M., Kljajević, L., Vukanac, I., Poznanović, M., Mihajlović-Radosavljević, A., Pavlović, V., 2012. Vertical distribution of natural radionuclides in soil: assessment of external exposure of population in cultivated and undisturbed areas. Sci. Total Environ. 429, 309–316. https://doi.org/10.1016/j.scitotenv.2012.04.054.

Padovani, S., Mitsios, I., Anagnostakis, M., Mostacci, D., 2018. Analysis of the vertical distribution and size fractionation of natural and artificial radionuclides in soils in the vicinity of hot springs. Radiat. Eff. Defect Solid 173 (9–10), 794–806. https://doi.org/10.1080/10420150.2018.1528605.

Pleiderer, S., Reitner, H., Heinrich, M., 2002. Zur Hydrogeologie der Kalkvoralpen nordöstlich der Enns (Oberösterreich), Beiträge zur Hydrogeologie/53/Seiten45-60/Graz.

Rosholt, J.N., 1983. Isotopic composition of uranium and thorium in crystalline rocks. J. Geophys. Res. 88 (No B9), 7315–7330.

Scarciglia, F., Nicolaci, A., Del Bianco, S., Pelle, T., Soligo, M., Tuccimei, P., Marzaioli, F., Passariello, I., Iovino, F., 2020. Reforestation and soil recovery in a Mediterranean mountain environment: insight into historical geomorphic and vegetation dynamics in the Sila Massif, Calabria, southern Italy. Catena 194, 104707. https://doi.org/10.1016/j.catena.2020.104707.

Sharma, D.A., Keesari, T., Rishi, M.S., Pant, D., 2018. A study on the role of hydrogeology on the distribution of uranium in alluvial aquifers of northwest India. Environ. Monit. Assess. 190, 746. https://doi.org/10.1007/s110661-018-7112-6.

Standortskarte, 2020 https://lfz.boku.ac.at/daten/Standortskarte.pdf (request from 4th November 2020).

Thørring, H., Wærsted, F.M., Raaness, A., Skipperud, L., Kiel Jensen, L., 2020. Elevated natural radioactivity in undisturbed forest and mountain areas of artic Norway – local geology, soil characteristics, and transfer to biota. J. Environ. Radioact. 222, 106291 https://doi.org/10.1016/j.jenvrad.2020.106291.

Vukašinović, I., Đorđević, A., Rajković, M., Todorović, D., Pavlović, V.B., 2010. Distribution of natural radionuclides in anthrosol-type soil. Turk. J. Agric. For. 24, 539–546. https://doi.org/10.3906/tar-0911-59.

Vukašinović, I., Todorović, D., Životić, Lj, Kaluđerovic, L., Đorđević, A., 2018. An analysis of naturally occurring radionuclides and ^{137}Cs in the soils of urban areas using gamma-ray spectrometry. Int. J. Environ. Sci. Technol. 15, 1049–1060. https://doi.org/10.1007/s13762-017-1467-z.